Mineralium Deposita (2020) 55:697–730
https://doi.org/10.1007/s00126-018-0813-5

ARTICLE

Paragonite-chloritoid alteration in the Trafalgar Fault and Fimiston- and Oroya-style gold lodes in the Paringa South mine, Golden Mile, Kalgoorlie: 2. Muscovite-pyrite and silica-chlorite-telluride ore deposited by two superimposed hydrothermal systems

Andreas G. Mueller[1]

Received: 9 October 2017 / Accepted: 20 May 2018 / Published online: 2 July 2018

Abstract

The Golden Mile deposit (1751 t Au to 2017) in the Archean Eastern Goldfields Province, Yilgarn Craton, Western Australia, is located in a km-scale envelope of chlorite-calcite-albite alteration overprinting metamorphosed tholeiitic rocks. The propylitic zone (310–340 °C) is centered on D2 strike-slip faults segmenting D1 folds. At the southeast margin of the deposit, 200 m wide hydrolytic paragonite-ankerite-chloritoid alteration (< 0.1 g/t Au) associated with the D2 Trafalgar Fault forms a thermal anomaly (405–425 °C). The Trafalgar alteration zone merges with barren ankerite-sericite replacement in propylitic Paringa Basalt bound to the contact with Golden Mile Dolerite, which extends > 1.5 km northwest to the Paringa South mine. In the mine, D2 faults control Fimiston ore locally overprinted by Oroya ore, whereas D3 reverse faults offsetting the D2-system control only Oroya ore. Representative ore bodies (lodes) were studied by petrographic, geochemical, and thermometric methods. Fimiston ore (4–20 g/t Au) is refractory, characterized by 10% pyrite ± chalcopyrite ± tennantite, and varies in oxidation state (magnetite stable to hematite stable). Gold and tellurides form inclusions in pyrite. In propylitic GMD, lode alteration is zoned from albite stable in veins and selvages (400 °C) to outer hydrolytic phengite-quartz-ankerite replacement (370 °C). The younger Oroya ore in D3 faults contains free gold and is oxidized (5 g/t Au; pyrite-hematite) or reduced (50–120 g/t Au; pyrite-pyrrhotite) close to carbonaceous black schist. Oroya Stage 1 silica-chlorite-siderite replacement (400–425 °C) and As-rich pyrite-arsenopyrite-sphalerite mineralization is crosscut by Stage 2 silica-ankerite fill (385 °C) and Sb-rich pyrite-tetrahedrite-telluride mineralization associated with vanadian muscovite. Mass-balance calculations indicate that the Oroya fluid carried higher concentrations of silica, Fe, V, Ni, and Te than the older Fimiston fluid.

Keywords Kalgoorlie · Golden Mile · Pyrite · Telluride · Gold

Introduction

The Golden Mile deposit is located at 30° 47′ south latitude and 121° 29′ east longitude in the Kalgoorlie mining district of the 2.7 Ga Eastern Goldfields Province, Yilgarn Craton, Western Australia (Fig. 1). Production is subdivided into underground (1893–1992, 105.6 Mt at 11.27 g/t Au) and open pit (1984–2017, 291 Mt at 1.93 g/t Au recovered grade). About 80–85% of the total gold occurs as inclusions (0.5–20 μm) in pyrite and 15–20% in free Au-Ag tellurides (Travis et al. 1971), the two types of ore commonly termed Fimiston- and Oroya-style, respectively (e.g., Hagemann and Cassidy 2000). The structural setting, broad alteration zones, and associated porphyry dykes of the giant deposit are described in Mueller (2017) as part of this issue with emphasis on the Paringa South mine.

Krusch (1903) and Lindgren (1906) recognized that the ore bodies (lodes) represent sericite-ankerite replacement zones in fractured shear zones defined by the amount of disseminated

Editorial handling: S. Hagemann

Electronic supplementary material The online version of this article (https://doi.org/10.1007/s00126-018-0813-5) contains supplementary material, which is available to authorized users.

✉ Andreas G. Mueller
andreasm@iinet.net.au

[1] Centre for Exploration Targeting, School of Earth and Environment, The University of Western Australia, 35 Stirling Highway, Perth, W.A. 6001, Australia

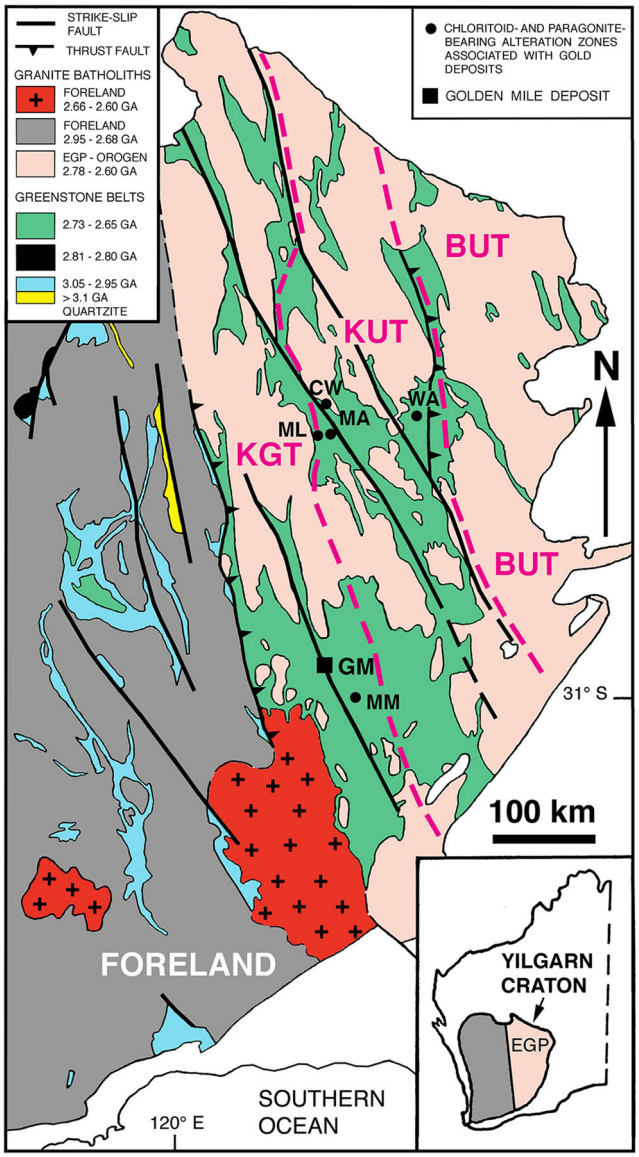

Fig. 1 Geologic map of the eastern Yilgarn Craton showing the 2.7 Ga Eastern Goldfields Province (EGP) subdivided into the Kalgoorlie Terrane (KGT) back-arc rift, the Kurnalpi Terrane (KUT) calc-alkaline magmatic arc, and the Burtville Terrane (BUT; after Cassidy et al. 2006). The continental foreland to the west contains greenstone belts and quartzites > 2.95 Ga old. The locations of the Golden Mile (GM) and other chloritoid-bearing alteration zones are shown. The inner zones at Mount Martin (MM), Mount Leonora (ML), and Mount Malcolm (MA) are characterized by the assemblage andalusite-kyanite ± sillimanite and, locally, by natro-alunite (Hallberg 1983; Purvis 1984). At Christmas Well (CW) and Wallaby (WA), inner pyrophyllite-sericite-quartz is present (Hallberg 1983; Mueller et al. 2008). Coordinates are latitude and longitude

pyrite. Simpson (1912) and Stillwell (1929) noted that the two largest ore bodies, the Horseshoe No. 3 and No. 4 lodes had central zones of chert-like silica. On levels of the Golden Horseshoe mine 90–244 m below surface, the siliceous core varied in thickness from 2.2 to 5.5 m and in average grade from 29 to 84 g/t gold (Krusch 1903). Tomich (1952, 1959) subdivided such replacement into early grey flint (3.4–5.2 g/t Au), and into late quartz breccia characterized by free gold, tellurides, and Green Leader vanadian muscovite. Sketches and photographs of individual lodes are in Larcombe (1913) and Clout et al. (1990).

Although the general nature of the lodes has been established, an integrated approach is lacking in previous studies. This one is the first combining structural mapping in the Paringa South underground mine, petrography, follow-up microscopy, and multi-element geochemistry to document ore bodies mined out during the recent open pit operation. Structural relations, silicate-carbonate, sulfide-oxide and sulfide-telluride assemblages, chlorite thermometry, and mass-balance calculations are employed to constrain the oxidation/sulfidation state of the ore and the local fluid evolution in space and time. This second contribution on the Paringa South mine precedes another two (this thematic issue) presenting electron microprobe analyses of gangue and ore minerals and related quantitative P-T-X constraints.

Pre-sulfide muscovite-paragonite-ankerite alteration bound to the contact Paringa Basalt-Golden Mile Dolerite extends from the mine southeast and merges with km-scale paragonite-ankerite-chloritoid alteration centered on the Trafalgar Fault. This zone, neglected since Prider (1947), is described in relation to propylitic alteration in the Golden Mile and discussed with respect to other chloritoid-bearing zones in the Eastern Goldfields Province containing pyrophyllite, kyanite and natro-alunite (Fig. 1).

Geologic setting

The Kalgoorlie district is located in the Eastern Goldfields Province (EGP) of the Yilgarn Craton, a continental-margin orogen characterized by 2.73–2.65 Ga greenstone belts. The EGP is composed of the Kalgoorlie, Kurnalpi, and Burtville Terranes (Fig. 1). The stratigraphic, structural, and magmatic-metamorphic evolution of the southern Kalgoorlie Terrane is reviewed in Mueller et al. (2016, this issue).

The lodes in the Golden Mile are confined to three stratigraphic units: the Paringa pillow basalt, the 600–750-m-thick Golden Mile Dolerite sill, and the Black Flag greywacke. The Golden Mile Dolerite (GMD), emplaced at the basalt-greywacke contact, is dated at 2685 ± 5 Ma (zircon U-Pb; Tripp 2013). The sill consists of ten petrographic units (Travis et al. 1971). The variolitic GMD units 1 and 10 represent the lower and upper chilled margins, units 2 and 3 are pyroxene-rich, and units 4, 5, and 9 are ophitic quartz gabbro. The central GMD units 6 to 8 differ due to abundant Ti-magnetite and ilmenite, and are interpreted to represent a pulse of iron-rich tholeiitic magma. The Paringa Basalt (PB), Golden Mile Dolerite, and Black Flag greywacke are folded into the Kalgoorlie Anticline and Syncline (D1) and

metamorphosed to the actinolite-albite-zoisite greenschist facies (e.g., Mueller 2017, this issue).

The Golden Mile deposit is controlled by the Boulder Lefroy-Golden Mile fault system (D2a), which displaces the regional upright folds (D1) 11–12 km in a left-lateral sense (Mueller et al. 2016, this issue). The steeply SW-dipping shear zones centered on the Golden Mile Fault, collectively termed the Fimiston Lodes, are bounded by the Boulder Lefroy Fault in the southwest and by the Trafalgar Fault in the northeast. The D2a Trafalgar Fault offsets the sub-vertical contact GMD-greywacke 660 m in a sinistral sense (Woodall 1965). Granodiorite porphyry dykes were emplaced into the fault system at 2676 ± 7 to 2671 ± 10 Ma after peak metamorphism but prior to hydrothermal chlorite-calcite alteration. Barren sericite-ankerite zones in the Golden Mile Fault and at the GMD-PB contact of the Kalgoorlie Anticline formed during the intrusion of diorite dykes at 2663 ± 11 Ma (Gauthier et al. 2007; Mueller 2017).

To the northwest, the Golden Mile deposit is displaced about 2 km at the north-striking dextral Golden Pike Fault (D4). Fimiston lodes northwest of this fault are characterized by laminated quartz veins and contain telluride shoots dominated by hessite causing low Au/Ag ratios (0.12–0.35) in the ore (Mueller and Muhling 2013). These peripheral lodes are not part of this study. They are offset at three closely spaced D4 faults, which control the quartz vein ore bodies of the Mt Charlotte deposit (151 t Au to 2017) dated at 2655 ± 13 to 2651 ± 9 Ma (xenotime U-Pb; Rasmussen et al. 2009; Mueller et al. 2016).

The Golden Mile lodes described below are ordered according to the time of formation of the host structure: D2a sinistral strike-slip faults (Fimiston system), D2b sinistral-reverse faults (Australia East system), and D3a reverse faults (Oroya system). The D2a and D2b faults formed in metamorphic rocks prior to the emplacement of granodiorite dykes at ca. 2675 Ma. Golden Mile hydrothermal activity was synchronous with D2c sinistral strike-slip reactivation and with D3a reverse faulting. It ceased before the development of barren D3b thrusts (Mueller 2017; this issue).

Methods and terminology

Selected ore bodies (B-Lode, Kelly Lode, Blatchford Lode, OHW Lode) on levels 4, 6, 7, and 11 of the Paringa South shaft were mapped by the author at scales of 1:12 to 1:25. The locations are shown on level plans in Mueller (2017; Figs. 8, 9, and 12), and are given below in mine grid coordinates. The Flat Lode stoped between the North Kalgurli shaft 13 and 14 levels is described based on reconnaissance sampling. In structural terms, the ore bodies represent altered shear zones composed of brittle fault-fill veins, extension veins, and breccia (Sibson 1977; Robert and Poulsen 2001) and of S-C mylonites characterized by recrystallized quartz and carbonate (Lister and Snoke 1984).

All samples were ground flat and examined (15–60× magnification). In 21 hand specimens, the short wavelength infrared (SWIR) absorption spectra (350–2500 nm) of white mica and chlorite were recorded with the TerraSpec™ instrument of Analytical Spectral Devices and interpreted using The Spectral Geologist™ software (Table 1). Gangue and ore minerals in 70 polished and covered thin sections and in 23 polished mounts were identified in transmitted and/or reflected polarized light. The covered thin sections were stained with Alizarin Red S + potassium ferricyanide solution. Stained calcite is red brown, ferroan calcite dark blue, dolomite is not stained, and ferroan dolomite is turquoise (Deer et al. 1992). In addition, cores from drill holes intersecting the Trafalgar Fault and 24 related thin sections (Prider 1947) stored at the Clarke Earth Science Museum of the University of Western Australia were re-examined.

The minerals in summary Tables 1 and 2 are named according to 768 wavelength dispersive analyses of silicates, carbonates and oxides, and 580 analyses of sulfides, tellurides, and gold acquired by the author using the JEOL JXA-8530F electron microprobe at the Centre for Microscopy, Characterization and Analysis, the University of Western Australia. Temperatures based on the $Al^{(IV)}$-in-chlorite thermometer of Cathelineau (1988) are reported for each mineralized structure (Table 1). The extension of this thermometer to 420 °C has been tested using the "average PT" approach in Thermocalc 3.26 (Powell and Holland 1994), the thermodynamic data in Holland and Powell (1998), and two chlorite-paragonite assemblages listed in the Electronic Supplementary Material (ESM App. 1 and 1a).

The term "silica" is used for chert-like quartz composed of minute granular crystals, and "chalcedony" for silica marked by pores and fibrous quartz (Deer et al. 2004). The term "sericite" denotes unidentified white mica, "phengite" is applied to muscovite with $^{[4]}Si > 3.1$, and "paragonite" to white mica with a ratio $K/(K + Na) < 0.2$ (Fleet 2003). The carbonates are subdivided by their $Mg/(Mg + Fe^{2+})$ ratio: dolomite > 0.8, ankerite 0.3 to 0.8, and siderite < 0.3 (Chang et al. 1998). Minerals in contact without evidence of reaction are considered in equilibrium and are hyphenated or joined with plus signs. Equilibrium assemblages constrain the local oxidation state (Frost 1991) and sulfidation state (Einaudi et al. 2003) of the ore bodies in f_{O2}-T and f_{S2}-T space, respectively (see footnote in Table 2).

Samples pulverized in agate or corundum mills were analyzed at the University of Western Australia for: (1) mineral composition by X-ray diffraction (XRD) and (2) whole-rock major and trace elements by X-ray fluorescence (XRF) using glass discs and pressed-powder pellets (Mueller 1990). Additional trace element analyses were carried out by fire assay, atomic absorption spectroscopy (AAS), and inductively

Table 1 Wall-rock alteration mineralogy, Trafalgar Fault and ore bodies (lodes) in the Paringa South and North Kalgurli mines, Golden Mile, Kalgoorlie

Structure (ore type)	Pre-sulfide host rock	Internal zones/structures	White mica	Chlorite	Chlorite *T* (°C) (analyses)	Carbonate	Other gangue minerals	Reference
Trafalgar Fault (< 0.1 g/t Au)	GMD Unit 9 Chlorite Albite Calcite ± epidote	Outer paragonite-ankerite zone	Paragonite, K/(K + Na) = 0.16, SWIR 2189.6–2190.5 nm	Minor, Mg # 0.21, V2O3 = 0.11 wt.%, SWIR 2262.2 nm	406 ± 50 (n = 16)	Ankerite Mg # 0.33	Chloritoid ± albite, rutile ± tourmaline	Fig. 2b, App. 1
		Inner paragonite-albite zone	Paragonite, XRD d001 = 9.61 Å, SWIR 2189.3 nm	Rare to minor		Ankerite	Chloritoid, albite ± rutile ± tourmaline ± epidote	Fig. 2b
Paringa B-Lode (Fimiston)	GMD Unit 4 Chlorite Albite Calcite	Inner phengite-albite selvage of veins	Phengite, K/(K + Na) = 0.94, SWIR 2205.8 nm	Absent		Ankerite Mg # 0.65	Albite ± rutile ± fluor-apatite	Fig. 4
		Outer phengite-ankerite zone	Phengite, K/(K + Na) = 0.96, SWIR 2204.3 nm	Minor, Mg # 0.46, V2O3 < 0.03 wt.%	371 ± 50 (n = 20)	Ankerite Mg # 0.56, Mg-rich rims	± albite, rutile	Fig. 4
Paringa Kelly Lode (Fimiston)	GMD Unit 2 Chlorite (Mg#0.5) SWIR 2255.1 nm Albite, Fe-calcite ± Si-muscovite	Inner muscovite-albite selvage of veins	Si-rich muscovite, K/(K + Na) = 0.89, SWIR 2202.5–2204.3 nm, XRD d001 = 9.98 Å	Rare (most in outer mottled selvage), SWIR 2254.7 nm	339 ± 50 (n = 18), remnant propylitic chlorite	Dolomite Mg # 0.93, ankerite Mg # 0.71	albite ± rutile ± tourmaline ± apatite	Fig. 6
Paringa Blatchford Lode (Fimiston and Oroya)	Pillowed PB Muscovite SWIR 2194.7 nm Ankerite ± chlorite SWIR 2261.2 nm ± albite, rutile	Early shear zone S-C mylonite (Fimiston)	Muscovite, K/(K + Na) = 0.73, SWIR 2195.4 nm	Absent		Ankerite Mg # 0.45	± tourmaline ± rutile	Fig. 9
		Intermediate shear zone replacement and fault breccia (Oroya Stage 1)	Minor muscovite	Major, Mg # 0.29, V2O3 = 0.05 wt.%	402 ± 50 (n = 15)	Ankerite Mg # 0.43, siderite, ± calcite	Chalcedony ± tourmaline ± rutile	Fig. 9
		Late telluride extension vein (Oroya Stages 1 + 2)	Si-rich muscovite, K/(K + Na) = 0.75–0.92, SWIR 2196.4–2197.3 nm, V2O3 = 2.4–8.5 wt.%	Rare, Mg # 0.10–0.14, Stage 2 has V2O3 = 2.0 wt.%	402 ± 50 (n = 4), for Stage 1 only	Fe-calcite, dolomite Mg # 0.96, ± ankerite ± siderite	Chalcedony ± rutile ± tourmaline ± apatite	Fig. 9
Paringa OHW Lode (Oroya)	Pillowed PB Muscovite XRD d001 = 9.90 Å Ankerite ± paragonite XRD d001 = 9.71 Å ± albite, rutile	Shear zone replacement and fill (Oroya Stage 1)	Minor muscovite, K/(K + Na) = 0.86, SWIR 2194.9–2195.7 nm, XRD d001 = 9.90 to 9.93 Å	Major, Mg # 0.26–0.49, V2O3 ≤ 0.2 wt.%, SWIR 2257.1–2260.9 nm	423 ± 50 (n = 20) to 413 ± 50 (n = 22)	Ankerite Mg # 0.62, siderite	Chalcedony ± tourmaline ± rutile	Fig. 13

Table 1 (continued)

Structure (ore type)	Pre-sulfide host rock	Internal zones/structures	White mica	Chlorite	Chlorite T (°C) (analyses)	Carbonate	Other gangue minerals	Reference
		Late telluride breccia and fill (Oroya Stage 2)	Minor muscovite, K/(K + Na) = 0.89, SWIR 2195.3 nm, V2O3 = 0.5–2.5 wt.%	Minor, Mg # 0.16–0.19, V2O3 = 0.2–1.4 wt.%	385 ± 50 (n = 6), only chlorite ≤ 0.2 wt.% V2O3	Ankerite Mg # 0.60, ± dolomite Mg # 0.83, ± siderite	Chalcedony ± V-tourmaline ± fluor-apatite ± rutile	Fig. 13
		Late extension veins (Oroya Stage 3)	Absent to rare	Minor Fe-chlorite		Ankerite, siderite		Fig. 13
North Kalgurli Flat Lode (Oroya)	GMD Unit 5? Chlorite Albite Calcite	Fault breccia and replacement (Oroya Stage 1)	Absent to rare muscovite?	Minor, Mg # 0.29, V2O3 = 0.10 wt.%	384 ± 50 (n = 11), in breccia cement	Siderite, ankerite Mg # 0.4–0.5	± chalcedony ± rutile	Fig. 15

The SWIR Al-OH absorption features at 2200 nm and 2250 nm define the white mica and chlorite compositions, respectively (Wang et al. 2017). The Mg-number (Mg #) is the ratio Mg/(Mg + Fe^{2+}). Quartz is present in all assemblages, chalcedony denotes chert-like microcrystalline quartz. The chlorite temperature is based on the empirical Al (IV) calibration of Cathelineau (1988). The 2-sigma error is estimated at ± 50 °C (Lanari et al. 2014). All chlorite electron microprobe analyses (≤ 0.2 wt.% V2O3) were normalized to 14 oxygens using the computer program AX of Holland and Powell (2000) after eliminating elements close to the detection limit (V, Ti, Ca, Na, K). In AX, Fe^{3+} is estimated from stoichiometry (> 10 cations) but all iron was ferrous

GMD Golden Mile Dolerite, *PB* Paringa Basalt, *prefix* ± accessory minerals, *SWIR* short-wave infrared absorption, *XRD* X-ray diffraction

coupled plasma mass spectrometry (ICP-MS) at Intertek-Genalysis, Perth. The analytical details are listed in ESM Appendix 2. A mill-head sample representing 210,410 t of Fimiston sulfide ore mined in 1985/86 from the Lake View and Perseverance shafts was also analyzed (Mueller 1990).

Paragonite-bearing replacement zones

In the Paringa South mine, barren muscovite-ankerite ± paragonite ± chlorite ± magnetite alteration overprints propylitic Paringa Basalt in a zone 150 m thick along the contact with Golden Mile Dolerite on the SW-limb of the Kalgoorlie Anticline (Figs. 2 and 3 in Mueller 2017, this issue). About 1.5 km southeast of the Paringa South shaft, the contact zone closes in the hinge of the anticline and merges with sub-economic paragonite-ankerite-chloritoid alteration in Golden Mile Dolerite centered on the Trafalgar Fault (Fig. 2a). Chloritoid occurs in a zone more than 240 m wide and 1000 m long (Prider 1947). Drill holes TRF-1 and TRF-2 intersect part of this zone (Fig. 2b). The presence of paragonite and chloritoid in barren alteration contrasts with the abundance of muscovite/phengite or chlorite in the ore bodies (Table 1). The paragonite-bearing replacement zones grade laterally into propylitic chlorite-calcite ± epidote alteration (Fig. 2a). In Golden Mile Dolerite, chlorite and Fe-calcite replace metamorphic actinolite and tschermakite in augite sites, and albite ± calcite ± sericite replace zoisite in plagioclase sites (Mueller 2017, this issue).

Trafalgar Fault: paragonite-ankerite zone

In the outer alteration zone of the Trafalgar Fault, the ophitic igneous texture of GMD Unit 9 is preserved (Fig. 3a). Microcrystalline ankerite, minor ferroan calcite, chlorite (3–10 vol.%), and magnetite form pseudomorphs after prismatic augite (1–4 mm). Lath-shaped albite is replaced by paragonite + quartz or, less commonly, by granular albite and quartz. Interstitial igneous quartz (1–3%) and trellised rutile lamellae after Ti-magnetite (2%) characterize GMD Unit 9 (Fig. 3a). Blue-grey chloritoid (1–5%) is in contact with Fe-chlorite, ankerite, paragonite, and quartz (Fig. 3b) and associated with trace tourmaline. Thermocalc temperature estimates vary from 396 ± 32 to 426 ± 34 °C (ESM App. 1a), and agree within error with chlorite thermometry (± 50 °C; Table 1). The zone contains disseminated early magnetite (0.5–2%), locally in contact with chloritoid (Fig. 3c), and late specular hematite, pyrite, chalcopyrite (Fig. 3d), and rare arsenopyrite. Some of the pyrite is zoned from poikilitic cores to solid rims.

Table 2 Mineral assemblages constraining the oxidation and sulfidation state of refractory Fimiston-style and subsequent non-refractory Oroya-style gold mineralization in ore bodies (lodes) of the Paringa South and North Kalgurli mines, Golden Mile, Kalgoorlie

Ore body (ore type)	Internal zones/structures	Gold grade Au/Ag ratio	Fe^{3+}/Fe^{2+} ratio	Sulfates, oxides (vol.%)	Sulfides (vol.%)	Tellurides, gold (vol.%)	Oxidation state	Sulfidation state
Paringa B-Lode (Fimiston)	Inner phengite-albite selvage of veins	4.7 g/t 0.43	0.24	3 magnetite (V) 3 hematite (Ti, V) 2 rutile	10 pyrite 0.1 chalcopyrite	< 0.1 hessite < 0.1 petzite < 0.1 coloradoite	High: hem-mag, hem rims mag	Intermediate: py-mag, py-hem-mag
	Outer phengite-ankerite zone		Not analyzed	3 magnetite 0.5 hematite 3 rutile	2 pyrite (As) 0.1 chalcopyrite < 0.1 tennantite < 0.1 cobaltite		High: hem rims mag	Intermediate: py-ccp-ten, py-mag
Paringa Kelly Lode (Fimiston)	Inner muscovite-albite selvage of veins	3.6 g/t 0.72	0.08	1 rutile	10 pyrite 0.1 chalcopyrite	< 0.1 petzite < 0.1 coloradoite < 0.1 melonite	Intermediate?	Intermediate: py-ccp
Paringa Blatchford Lode (Fimiston and Oroya)	Early shear zone S-C mylonite (Fimiston)	20 g/t	Not analyzed	2–3 rutile < 0.1 barite	10 pyrite (As) 0.2 chalcopyrite	< 0.1 gold	Intermediate?	Intermediate: py-ccp
	Intermediate shear zone replacement and fault breccia (Oroya Stage 1)	Not analyzed	Not analyzed	1–5 rutile	7–15 pyrite 1–3 pyrrhotite 0.3 arsenopyrite 0.5 chalcopyrite 0.5 sphalerite < 0.1 ullmannite		Low?	Low: py-po-asp
	Late telluride extension vein (Oroya Stage 1 and 2)	120 g/t 3.75	0.03	0.5 rutile (V)	3–10 pyrite 0.5–2 pyrrhotite 0.5 arsenopyrite 0.5 sphalerite 0.5 chalcopyrite 0.2 tetrahedrite < 0.1 bn-cv-dg	0.2 gold 0.5 montbrayite < 0.1 calaverite 0.1 petzite 0.1 altaite 0.1 tellurantimony 0.1 coloradoite 0.1 melonite	Low to intermediate?	Stage 1 low: py-po-asp Stage 2 intermediate to high: ccp-tth, cv-dg
Paringa OHW Lode (Oroya)	Shear zone replacement and fill (Oroya Stage 1)	48 g/t 16.0 (Oroya Stages 1 + 2)	0.03	0.5 rutile	10–15 pyrite 1 arsenopyrite 1 sphalerite 0.2 chalcopyrite < 0.1 pyrrhotite < 0.1 gersdorffite	< 0.1 gold < 0.1 melonite < 0.1 coloradoite	Low?	Low to intermediate: py-asp ± po, asp-ccp
	Late telluride breccia and fill (Oroya Stage 2)	Part of bulk sample	0.03	0.3 rutile	3–5 pyrite 0.5 sphalerite 0.2 chalcopyrite < 0.1 cv-dg (rim ccp) 0.1 arsenopyrite	0.3 gold 0.5–1 montbrayite 0.1 calaverite 0.2 tellurantimony 0.5 coloradoite 0.2 altaite	Low to intermediate?	Intermediate to high: py-ccp, cv-dg
	Late extension veins (Oroya Stage 3)	Not analyzed	Not analyzed	0.1 rutile	5 pyrite 2 sphalerite 0.5 arsenopyrite	0.2 gold	Low to intermediate?	Intermediate: py-asp
Nth Kalgurli Flat Lode (Oroya)	Fault breccia and replacement (Oroya Stage 1)	5 g/t	Not analyzed	5–7 magnetite (V) 2 hematite (Ti, V) 0.5 rutile	5 pyrite (As) 0.2 chalcopyrite	0.1 gold	High: hem rims mag	Intermediate: py-hem, py-mag

Ore mineral abundances are percent visual estimates based on hand specimen microscopy and thin-section transmitted/reflected light microscopy. Data for whole-rock Au/Ag and Fe^{3+}/Fe^{2+} ratios are in Table 3. Minerals: arsenopyrite (asp), bornite (bn), chalcopyrite (ccp), covellite (cv), digenite (dg), hematite (hem), magnetite (mag), pyrrhotite (po), pyrite (py), tennantite (ten), tetrahedrite (tth). The tellurides in refractory Fimiston ore occur as 0.5–5 μm inclusions in pyrite. Minerals in equilibrium contact are hyphenated. Oxidation state at 350–400 °C is constrained by the hematite-magnetite (HM) and fayalite-magnetite-quartz (FMQ) buffers to high (hematite stable), intermediate (magnetite stable), and low (ferrous iron in silicate, carbonate, pyrrhotite). The Fe^{3+}/Fe^{2+} ratio of the ore is not a quantitative measure of oxygen fugacity (Frost 1991). The sulfidation state is estimated according to sulfide-sulfide and sulfide-oxide reactions in fugacity-temperature diagrams in Einaudi et al. (2003; their Figs. 1 and 4)

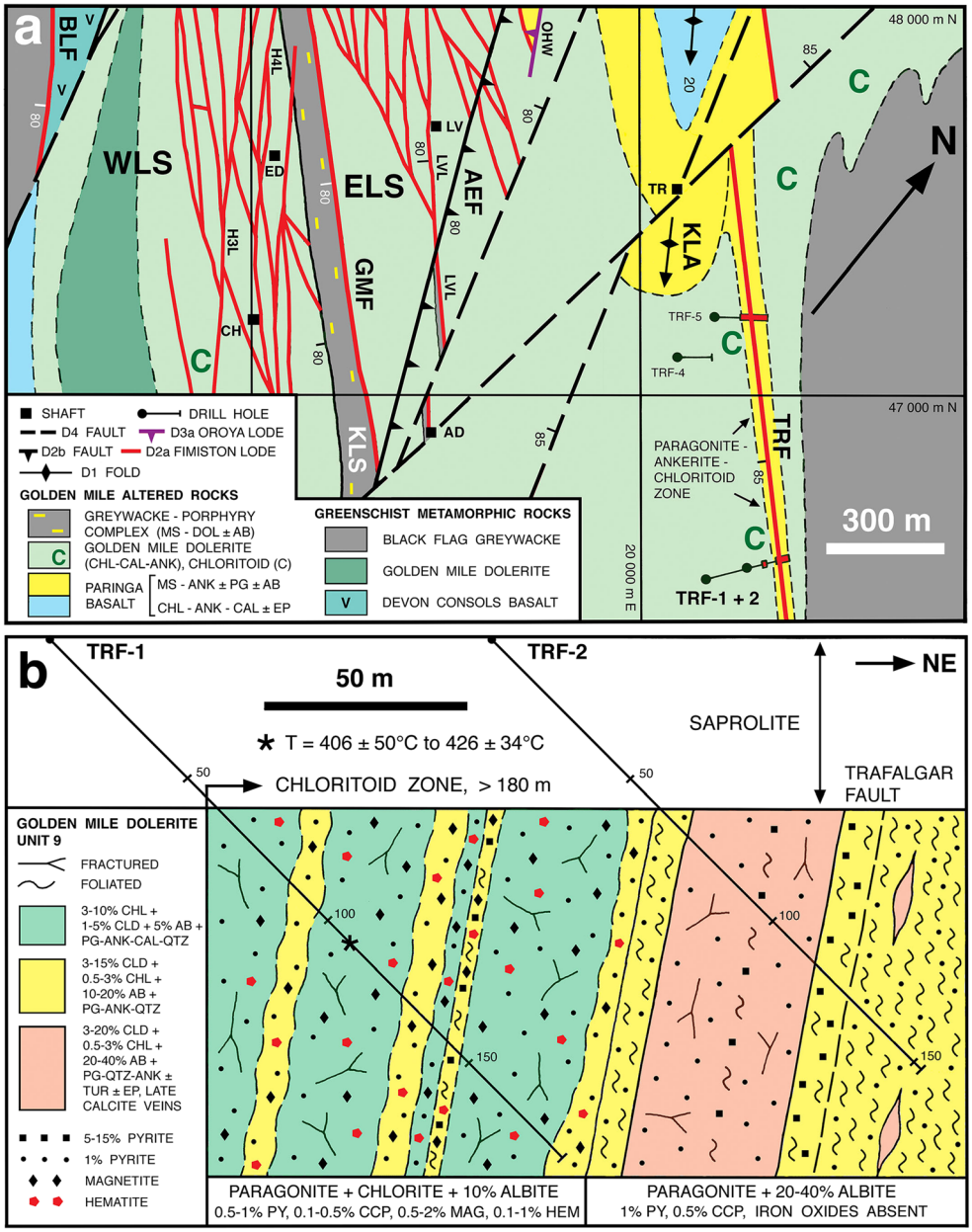

Fig. 2 Chloritoid-bearing paragonite-ankerite alteration associated with the D2a Trafalgar Fault, Golden Mile deposit, Kalgoorlie. **a** Structural plan at 300 m above sea level showing the southeast part of the Western and Eastern System of D2a Fimiston Lodes (WLS, ELS), the km-scale chloritoid zone (C), and the location of the Trafalgar drill holes (TRF). D1 folds: Kalgoorlie Anticline (KLA), Kalgoorlie Syncline (KLS). D2a sinistral strike-slip faults: Boulder Lefroy (BLF), Golden Mile (GMF), Trafalgar (TRF). D2a lodes: Horseshoe No. 3 (H3L), Horseshoe No. 4 (H4L), Lake View (LVL). D2b faults: Australia East (AEF). D3a reverse faults: Oroya Hanging Wall Lode (OHW). Shafts: Adelaide (AD), Chaffers (CH), Edwards (ED), Lake View Main (LV), Trafalgar (TR). **b** Northeast-southwest cross section through the chloritoid-bearing paragonite-ankerite alteration zone of the Trafalgar Fault based on the re-logging of diamond drill holes TRF-1 and TRF-2 (see **a**). Minerals: albite (ab), ankerite (ank), calcite (cal), chalcopyrite (ccp), chlorite (chl), chloritoid (cld), epidote (ep), hematite (hem), magnetite (mag), quartz (qtz), paragonite (pg), pyrite (py), tourmaline (tur)

Trafalgar Fault: paragonite-albite zone

The inner alteration zone centered on the Trafalgar Fault consists of paragonite-quartz-ankerite schist representing the ductile shear zone and of massive to weakly foliated albite-quartz-ankerite rock (Fig. 2b). Microcrystalline albite constitutes 10–20 vol.% of the schist and 20–40% of the massive rock. The greater abundance of albite and the scarcity of chlorite (about 3%) distinguish the inner from the outer zone. Chloritoid (5–10%, locally 20%) forms fan- or rosette-shaped aggregates (Fig. 3e). Tourmaline and apatite are accessories (Fig. 3f) but magnetite and hematite are absent. Clinozoisite-epidote (up to 5%) is part of the paragonite-albite assemblage locally (Fig. 3g). Subhedral pyrite (10–250 μm) is abundant in spaced zones (5–15%), where it forms aggregates with accessory chalcopyrite and gersdorffite (Fig. 3h). A bulk sample (TRF-2, 126–152 m) contained 75 ppb gold (ESM App. 2b).

Remnant ophitic texture defined by lath-shaped paragonite-quartz pseudomorphs, enclosed in igneous quartz (1–3 vol.%) and in trellised rutile lamellae (1–5 mm), is preserved in the albite-rich rocks. These are crosscut by calcite-ankerite veinlets and by banded veins up to 2 cm thick. The veins are zoned from chloritoid margins to cores of quartz and sparry ankerite and contain accessory pyrite and rutile.

In the schist, primary textures are obliterated and rutile forms granular streaks parallel to foliation. Seams of fine-grained paragonite wrap microcrystalline quartz-albite-ankerite aggregates. Tourmaline needles and a few chloritoid crystals are

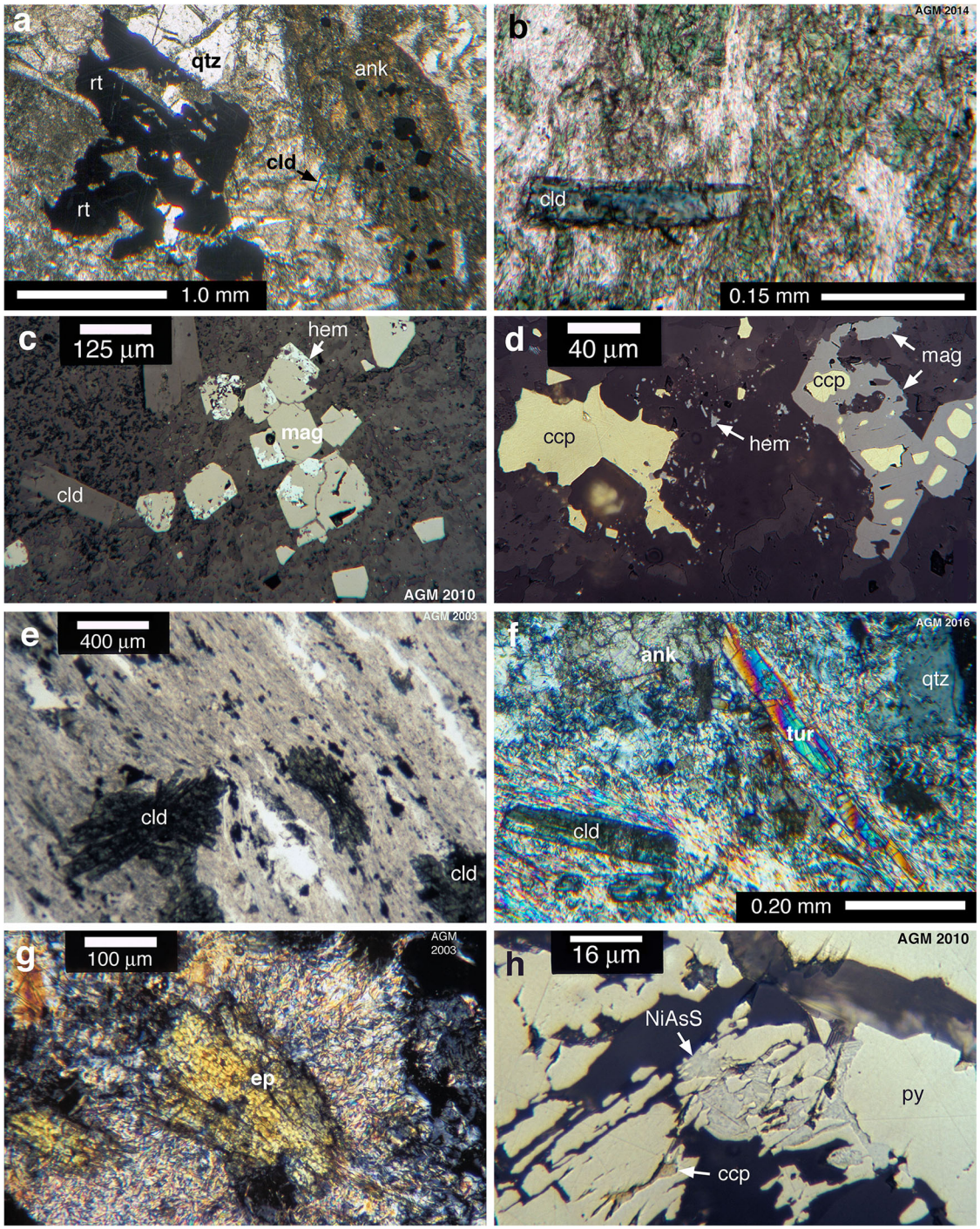

Fig. 3 Textures and chloritoid-bearing mineral assemblages in the outer paragonite-ankerite **(a–d)** and inner paragonite-albite **(e–h)** alteration zone of the D2a Trafalgar Fault, drill holes TRF-1 and TRF-2, southeast Golden Mile. The host rock is propylitic Golden Mile Dolerite (GMD) Unit 9. **a** Ophitic texture defined by ankerite (ank) + opaque magnetite in augite sites and by paragonite + quartz ± albite in plagioclase sites. Igneous quartz (qtz), chloritoid (cld), and rutile (rt) after Ti-magnetite are accessory. TRF-1, 96.3 m, plane polarized light. **b** Post-kinematic chloritoid (cld) in contact with Fe-chlorite (green) in a paragonite-quartz-ankerite matrix. TRF-1, 107.6 m, plane polarized light. **c** Magnetite (mag) rimmed by late hematite (hem) is in contact with tabular chloritoid (cld) in a matrix of ankerite, quartz, and paragonite. TRF-1, 96.3 m, plane polarized light reflected in air. **d** Magnetite (mag) partly replaced by chalcopyrite (ccp), adjacent chalcopyrite is in contact with hematite (hem) in quartz-ankerite ± paragonite groundmass. TRF-1, 96.3 m, plane polarized light reflected in air. **e** Post-kinematic chloritoid (cld) in paragonite-quartz S-C mylonite containing quartz-albite lenses (white) and opaque rutile. TRF-2, 145.7 m, plane polarized light. **f** Tourmaline (tur) aligned in the paragonite foliation adjacent to chloritoid (cld), ankerite (ank), and quartz (qtz). TRF-2, 89.0 m, crossed polarized light. **g** Clinozoisite-epidote (ep) in paragonite-albite-quartz ± rutile groundmass. TRF-3, 57.9 m, crossed polarized light. **h** Pyrite (py) in contact with chalcopyrite (ccp) and an isotropic mineral, probably gersdorffite (NiAsS). TRF-2, 107.0 m, plane polarized light reflected in air

fractured and pulled apart. Pressure shadows of paragonite and ankerite are common at chloritoid and pyrite crystals. Some paragonite plates and most chloritoid aggregates are post-kinematic and oriented at a high angle to the foliation (Fig. 3e).

Contact zone in Paringa Basalt

Pillows on the Paringa South shaft 6 level (49,320 m N, 19,905 m E), about 5 m below the GMD contact, consist of the alteration assemblage ankerite-quartz, minor white mica and albite, and rare rutile and chlorite. The XRD {001} peak of mica is split into two maxima, one at 9.90 Å and the other at 9.71 Å indicating muscovite interlayered with paragonite. Pillow basalt hosting the Blatchford Lode above the Paringa South shaft 11 level, about 30 m below the GMD contact, is composed of the same minerals except that the mica is muscovite (d_{001} = 9.97 Å). Granular rutile (1–15 μm) is disseminated (3 vol.%) but trellised rutile after Ti-magnetite is absent. Micro-phenocrysts and rare glomerocrysts of plagioclase (1–5%) are pseudomorphed by granular albite ± quartz and embayed by ankerite and muscovite.

The barren alteration zone also overprints two NW-striking quartz diorite dykes crosscutting Paringa Basalt (Fig. 16 in Mueller 2017). They display progressive replacement of albite by muscovite + quartz ± dolomite from the center to the margin: the whole-rock K_2O/Na_2O ratio increases from 1.64 to 6.67, and inner chlorite after hornblende changes to outer muscovite-ankerite pseudomorphs (Stillwell 1929).

Contact zone in GMD Unit 1

The main crosscut on the Paringa South shaft 7 level exposes Golden Mile Dolerite Unit 1 in contact with altered Paringa Basalt. The unit is characterized by orbicular albite-ankerite aggregates (5 mm) and by trellised rutile lamellae after Ti-magnetite (0.5 mm). Grains of igneous quartz (1 vol.%) and apatite (0.5%) are preserved. The GMD 10 m southwest of the PB contact consists of paragonite (30%), quartz (15%), albite (10%), ankerite (25%), chlorite (15%), and rutile (2%). Paragonite and quartz replace albite in lath-shaped sites. Ankerite and chlorite are pseudomorph after prismatic augite (0.5–1 mm). The paragonite XRD {001} peak at 9.67 Å indicates minor phengite interlayers. Chlorite thermometry (370 ± 50 °C) is consistent with Thermocalc estimates of 357 ± 54 °C to 394 ± 50 °C (ESM App. 1/1a).

Fimiston lodes in the Paringa South mine

Fimiston-style refractory ore accounts for 80–85% of the gold in the deposit (Travis et al. 1971), mostly controlled by D2a shear zones dipping steeply southwest (Fig. 2a). In the Paringa South mine, the B-Lode and Kelly Lode are representative of Fimiston-style ore. A post-porphyry phase of syn-mineralization (D2c) sinistral slip along a line pitching 10–20° SE is recorded on the Kelly Lode (Mueller 2017, this issue).

Paringa B-Lode

The B-Lode was mapped on the Paringa South shaft 6 level (194 m above sea level) in the 602 stope (48,900 m N; 19,605 m E). Quartz-ankerite ± pyrite veins 0.2–3 cm thick control red replacement selvages 5–15 cm wide, which grade outward into green-grey GMD Unit 4 (Fig. 4). The white mica

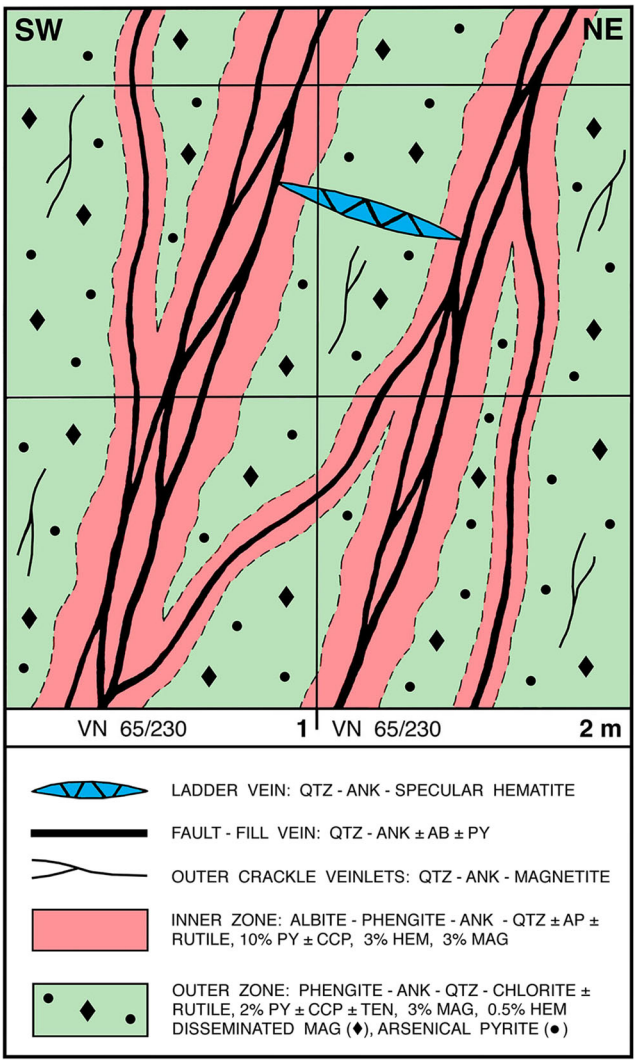

Fig. 4 Northeast-southwest cross section through the B-Lode, Paringa South shaft 6 level, 602 stope, the host rock is Golden Mile Dolerite Unit 4. The fault-fill veins are surrounded by red phengite-albite replacement selvages colored by dispersed hematite, and zoned from inner pyrite > magnetite to outer magnetite > pyrite. The phengite-ankerite zone contains minor chlorite (5%), magnetite (3%) rimmed by hematite, and aggregates (2%) of arsenical pyrite, chalcopyrite, tennantite, and cobaltite. Vein (VN) structural data are dip angle + dip direction. Minerals: albite (ab), ankerite (ank), apatite (ap), chalcopyrite (ccp), hematite (hem), magnetite (mag), pyrite (py), quartz (qtz), tennantite (ten)

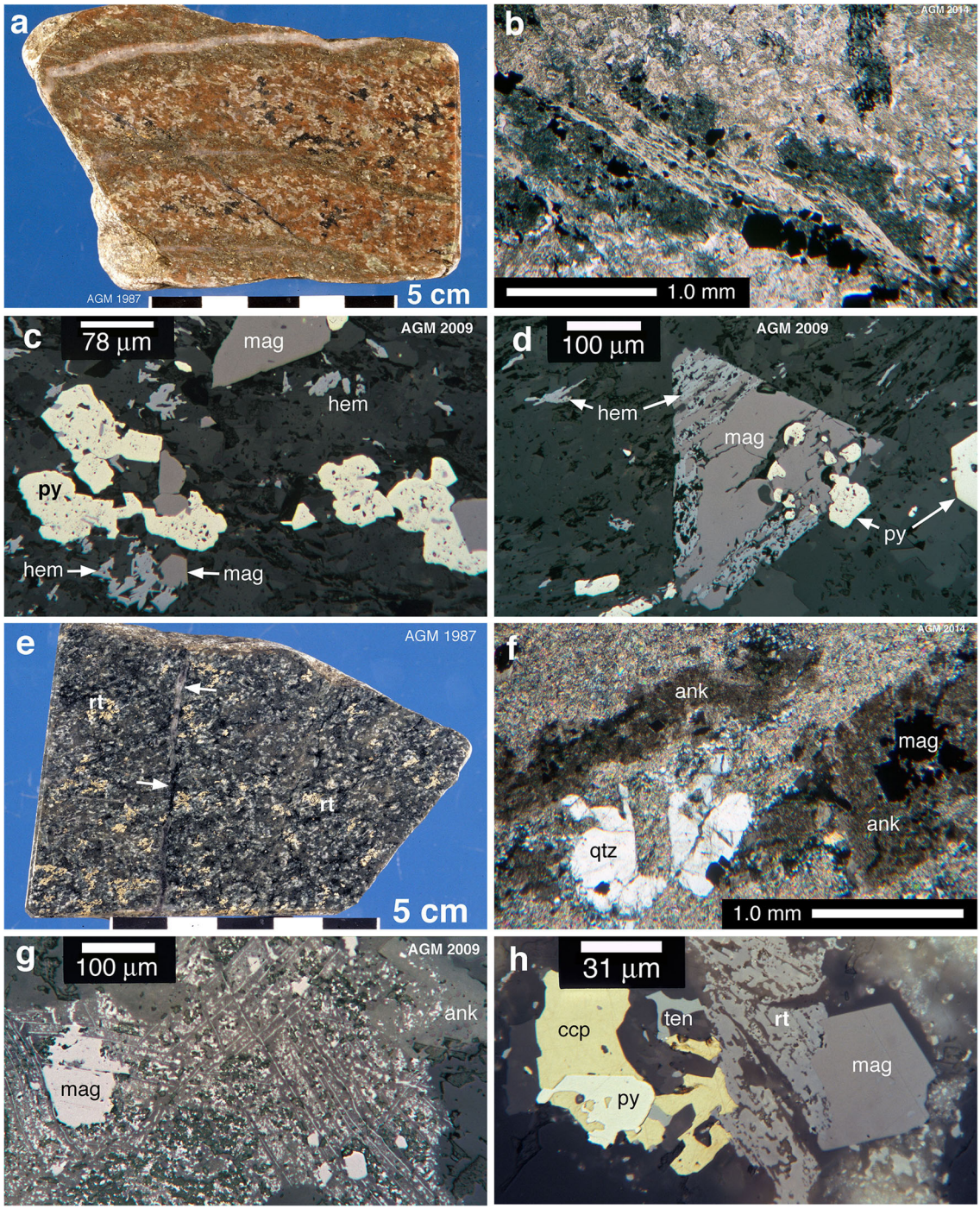

Fig. 5 Textures and mineral assemblages in the inner phengite-albite **(a–d)** and outer phengite-ankerite zone **(e–h)** of the B-Lode, Paringa South shaft 6 level, 602 stope. The host rock is Golden Mile Dolerite (GMD) Unit 4. **a** Grey quartz veins in red phengite-quartz-hematite rock mottled by grey albite-ankerite aggregates. The veins control selvages of auriferous pyrite (10–15 vol.%). Magnetite is rare close to veins and rimmed by pyrite at greater distance. **b** Vein-parallel phengite seam in a matrix of albite, quartz, ankerite (stained blue), and opaque pyrite. Remnant augite sites are filled with ankerite ± rutile ± hematite, plane polarized light. **c** Equilibrium assemblage pyrite-magnetite-hematite: magnetite (mag) in contact with pyrite containing hematite inclusions, and both pyrite (py) and magnetite in contact with specular hematite (hem). Plane polarized light reflected in air. **d** Magnetite (mag) in contact with pyrite is partly replaced by hematite (hem); the pyrite (py) does not contain hematite inclusions. Plane polarized light reflected in air. **e** Outer GMD Unit 4: pink rutile (rt) lamellae tracing Ti-magnetite. Augite sites are pseudomorphed by ankerite ± chlorite and feldspar sites by phengite + quartz ± albite. Quartz-magnetite veinlets cut across (arrows). **f** Augite sites filled with ankerite (ank), minor magnetite (mag), and chlorite. Plagioclase laths, outlined in igneous quartz (qtz), are replaced by phengite + quartz ± albite. Crossed polarized light. **g** Fine rutile lamellae (light grey) trace igneous Ti-magnetite replaced by chlorite (green), ankerite (ank), and magnetite (mag). Plane polarized light reflected in air. **h** Equilibrium assemblage chalcopyrite (ccp) + tennantite (ten) + arsenical pyrite (py) in contact with rutile (rt) replaced by magnetite (mag). Plane polarized light reflected in air

is phengite (Table 1). The red selvages are marked by phengite seams sub-parallel to the veins. Quartz-ankerite ladder veinlets connect the seams, and ladder veins filled with quartz, ankerite and specular hematite connect the main fault-fill veins. The outer GMD contains crackle fractures lined with magnetite and chlorite, and veinlets filled with quartz, albite, ankerite, and magnetite. Both form a network roughly parallel to the lode orientation (Fig. 4).

Inner phengite-albite zone The red selvage (Fig. 5a) is composed of heterogranular albite (35–40 vol.%), phengite (20%), ankerite (15–20%), quartz (10%), rutile lamellae after Ti-magnetite (2%; 0.5–3 mm), and fluor-apatite (0.5%). Most textures are secondary (Fig. 5b). Fine-grained hematite (3.97 wt.% TiO_2; 0.51% V_2O_3) and pyrite occur disseminated throughout, and magnetite is rare in a 0.5–5 cm wide zone bordering the veins (Fig. 5a). Pyrite decreases outwards giving way to disseminated magnetite (0.34 wt.% V_2O_3). Although magnetite, hematite, and pyrite are locally in equilibrium (Fig. 5c), defining a high oxidation and an intermediate sulfidation state (Table 2), hematite and pyrite also rim and partly replace magnetite (Fig. 5d). The pyrite contains inclusions (1–5 μm) of hematite, chalcopyrite, coloradoite, hessite, and petzite. The Au/Ag ratio of the ore is low (Table 2).

Outer phengite-ankerite zone The outer GMD Unit 4 is characterized by disseminated aggregates of pale brown trellised rutile tracing grains (2–7 mm) of Ti-magnetite (Fig. 5e). Other igneous textures are pseudomorphs after prismatic augite or lath-shaped plagioclase (Fig. 5f) and interstitial grains of quartz (2%) enclosing apatite needles. The augite sites (about 35 vol.%) are replaced by ankerite, and by minor chlorite and subhedral magnetite (0.12 wt.% V_2O_3). The plagioclase sites (50%) consist of phengite and minor granular quartz and albite (5–10%). Secondary magnetite (0.1–1 mm) replaces chlorite and ankerite in trellised rutile (Fig. 5g), and specular hematite rims magnetite locally. Sulfide aggregates are composed of arsenical pyrite, chalcopyrite, tennantite (Fig. 5h), and rare cobaltite (Table 2).

The average composition of the altered rock in the phengite-ankerite zone is 5 vol.% chlorite, 45% phengite, 25% ankerite, 10% quartz, 5–10% albite, and 3% rutile. In contrast, chlorite-calcite altered GMD Unit 4 exposed on the Perseverance shaft 23 level consists of 25% chlorite, 2% epidote, 25% calcite, 30% albite, 2% quartz, 3% rutile, and 7% sericite, the latter replacing plagioclase laths. The change in composition and a temperature gradient indicate that the phengite-ankerite zone of the B-Lode (370 °C) overprints outer chlorite-calcite alteration (340 °C; Table 1).

Paringa Kelly Lode

The Kelly Lode was mapped parallel to strike on the Paringa South shaft 4 level (255 m above sea level) in the east wall of the drive at 49,275 m north and 19,707 m east. The section illustrates the termination of the lode to the southeast (Fig. 6). A thick brecciated fault-fill vein marks the footwall boundary, and a parallel array of thinner veins extends into the hanging wall. Channel samples cut across the footwall vein indicate

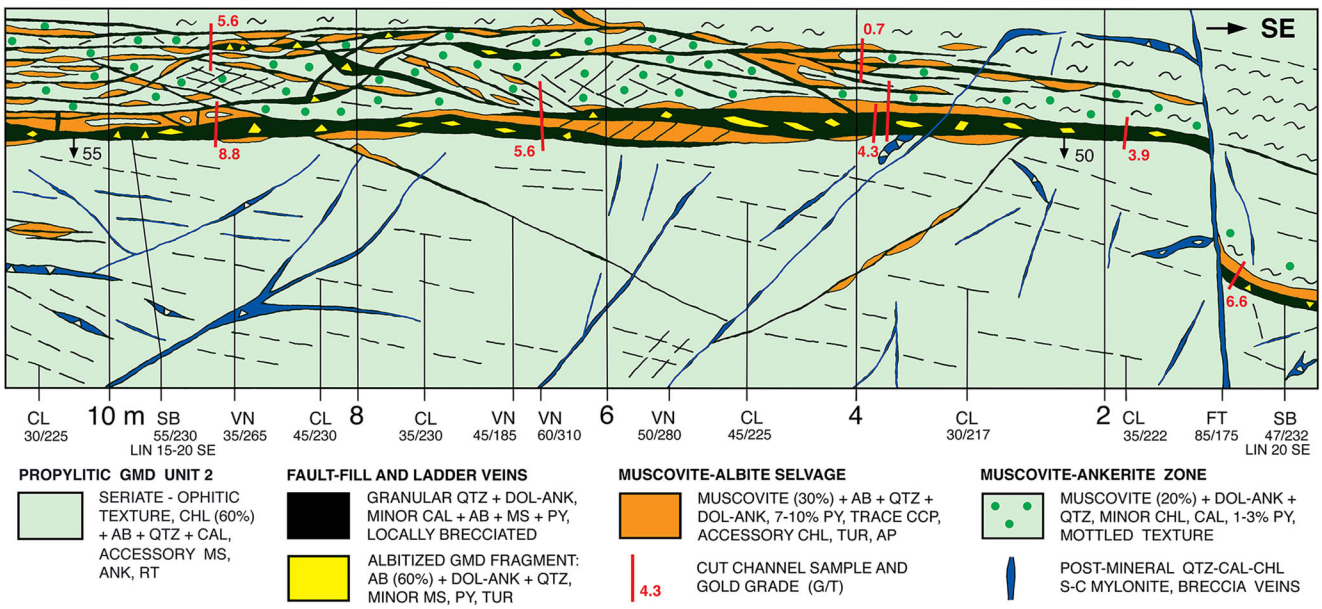

Fig. 6 Northwest-southeast section parallel to strike of the Kelly Lode, Paringa South shaft 4 level, looking northeast at the wall of the drive. The host rock is Golden Mile Dolerite Unit 2. The section illustrates the termination of the lode to the southeast. The muscovite-albite-pyrite replacement selvages of the veins lack magnetite and hematite. Structural data are dip angle + dip direction. Structures: cleavage (CL), fault (FT), lineation (LIN), shear-zone boundary (SB), vein (VN). Minerals: albite (ab), ankerite (ank), apatite (ap), calcite (cal), chalcopyrite (ccp), chlorite (chl), dolomite (dol), muscovite (ms), pyrite (py), quartz (qtz), rutile (rt), tourmaline (tur)

grades of 3.9 to 8.8 g/t gold, higher than those in the hanging wall array at the same northing (Fig. 6). The host rock is chlorite-calcite altered GMD Unit 2.

Fault-fill and ladder veins The footwall boundary vein is up to 15 cm thick and composed of heterogranular fill, microbrecciated fill, and breccia (Fig. 7a). Heterogranular fill (0.1–3 mm) consists of strained quartz crystals (10–90 vol.%), dolomite zoned to ankerite rims (5–60%), ferroan calcite (1–20%), albite (1–10%), muscovite (2–5%), pyrite (1–3%), and accessory (0.5%) tourmaline, chlorite, rutile, apatite, and chalcopyrite. In places, quartz-ankerite cement encloses angular vein fragments (Fig. 7b) of quartz ± carbonate or quartz-albite-muscovite. Wall-rock fragments (0.5–10 cm) are replaced by twinned albite (Fig. 7c), zoned dolomite-ankerite (10–30%), quartz (5–30%), muscovite (2–15%), and pyrite (2–7%). Some are rimmed by tourmaline (1–5%). Late breccia at the footwall contact contains fragments of chloritic GMD Unit 2 (Fig. 7a) cemented by dolomite, ankerite, and Fe-calcite. The carbonates form bands of granular or comb-textured crystals alternating with bands of quartz, albite, and muscovite. The fault-fill veins in the hanging wall (Fig. 6) are mostly 2–10 mm thick, similar in mineralogy to the main vein, and linked by quartz-carbonate ladder and crackle veinlets. Ladder veinlets are characterized by muscovite and chlorite plates oriented perpendicular to the walls and, locally, by selvages of disseminated tourmaline.

Vein replacement selvages Pyrite-rich selvages extend 0.5–10 cm from the veins (Fig. 6) grading first into wall rock mottled by cm-sized chloritic domains and then into chlorite-calcite altered GMD Unit 2. The fine-grained inner zone consists of phengitic muscovite (15–40 vol.%), granular quartz and albite (25–45%), dolomite and ankerite (25–35%), pyrite (10%), trellised rutile (0.2–1 mm), and accessory (0.3–2%) chlorite, tourmaline, and apatite (Tables 1 and 2). Igneous textures are not preserved (Fig. 7d). Vein-parallel muscovite seams are present, and some pyrite crystals have muscovite-quartz pressure shadows but are not rotated. Chlorite in contact with pyrite crystallized at 390–400 °C. Pyrite contains inclusions of chalcopyrite (Fig. 7e) and micron-sized grains of coloradoite, melonite, and petzite. Iron oxides are absent. The whole-rock Fe^{3+}/Fe^{2+} ratio is lower than in the B-Lode (Table 2).

In the chlorite-mottled transition zone, the amount of disseminated pyrite decreases gradually to about 1% and the igneous ophitic texture is partly preserved (Fig. 7f). The chlorite is remnant and has the same SWIR absorption and temperature estimate (340 °C) as chlorite in the footwall of the lode (Table 1). Augite sites (0.5–3 mm) consist of ankerite (40–50%), dolomite (20–30%), chlorite (5–25%), muscovite (5–10%), and rutile (0.5%). Felsic sites after lath-shaped plagioclase (0.2–1.5 mm) are composed of muscovite (30%), granular quartz and albite (55%), and calcite (5%). Rutile forms lamellae after Ti-magnetite.

Chlorite-calcite altered GMD Unit 2 The GMD in the footwall of the lode is composed of chlorite (60 vol.%), granular quartz and albite (15%), lath-shaped albite (10%), ferroan calcite (10%), muscovite and ankerite (3%), unstrained rutile trellis after Ti-magnetite (0.1–0.8 mm), and trace pyrite and chalcopyrite (0.1%). Igneous quartz is absent. Augite crystals up to 5 mm long are replaced by chlorite (Fig. 7g) and by remnant metamorphic actinolite needles (0.5%). Albite laths (0.2–0.7 mm) are enclosed in chlorite-calcite aggregates after augite interstitial to the larger crystals. Calcite is zoned to iron-rich rims (Fig. 7h).

Post-mineral fault and veins A barren fault marked by a narrow quartz-calcite-chlorite S-C mylonite offsets the lode at the southeast end of the section mapped. The fault strikes N85°E, dips 85°S, and is associated with quartz-calcite breccia veins. Drag on the boundary vein of the lode indicates a south side down component of movement (Fig. 6).

Fimiston and Oroya ore in the Blatchford Lode

Oroya-style pyrite-telluride ore, visually characterized by chert-like silica and chlorite, overprints Fimiston refractory ore in the central part of D2a shear zones and in sinistral-reverse D2b faults of the Australia East system. The principal mineralized D2b fault in the Paringa South mine is the Blatchford Lode, which forms narrow (1 m) tabular ore bodies in chlorite-calcite altered Golden Mile Dolerite and wide (6 m) pipe-shaped breccia ore in sericite-ankerite altered Paringa Basalt close to the hinge of the Brownhill Syncline (Fig. 8a), a subsidiary fold of the Kalgoorlie Anticline (Mueller 2017, this issue).

Lenses of sheared and altered Black Flag greywacke (Fig. 8b), thickened in the hinge of the syncline, contain carbonaceous matter (5–10 wt.% carbon). In 1905, methane was encountered in silica-chlorite-ankerite breccia intersected by a drill hole inclined from the − 320 m level of the Iron Duke shaft (Fig. 8a). The gas escaped over 2 days (Montgomery 1906). The occurrence suggests that organic methane trapped in local fault zones played a reducing role during gold mineralization.

The Blatchford breccia ore is characterized by Oroya-style chlorite-ankerite-quartz alteration and pyrite-sphalerite-chalcopyrite mineralization (Fig. 8c). Late Green Leader quartz veins (0.5–3 cm) marked by selvages of disseminated arsenopyrite and mineralized with native gold, petzite, coloradoite, melonite, altaite, and native tellurium (as inclusion in altaite) were mined on the Paringa South shaft 9 and 10 levels. The veins persisted into the Blatchford shear zone above the GMD-PB contact but decreased upwards and gave way to Fimiston-style pyrite ore (Scantlebury 1983).

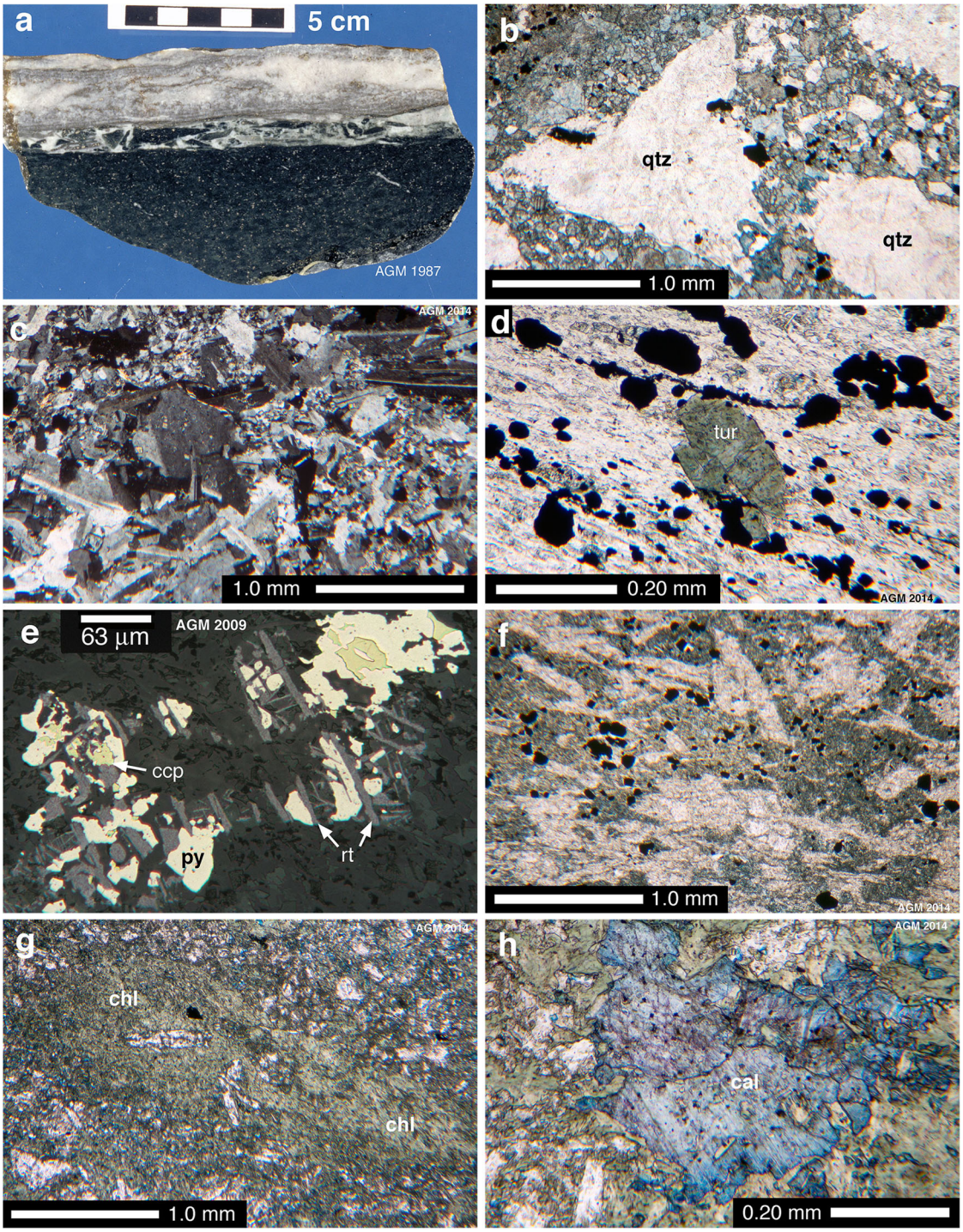

Fig. 7 Textures and mineral assemblages in the Kelly Lode, Paringa South shaft 4 level, Kelly drive. The host rock is propylitic Golden Mile Dolerite (GMD) Unit 2. **a** Footwall fault-fill vein composed of quartz, Fe-dolomite and Fe-calcite (tarnished brown), minor albite, tourmaline, and pyrite. At the contact: green fragments of GMD and older vein fill cemented by banded Fe-dolomite and Fe-calcite. GMD below: chlorite pseudomorphs after augite and pink rutile after Ti-magnetite. **b** Footwall fault-fill vein: fragments of granular vein quartz (qtz) in a matrix of ankerite (stained light blue), quartz, and Fe-calcite (dark blue), plane polarized light. **c** Footwall fault-fill vein: GMD fragment replaced by albite (twinned) and trace muscovite, crossed polarized light. **d** Inner vein selvage: muscovite-quartz-albite ± ankerite schist, non-rotated opaque pyrite and tourmaline (tur), plane polarized light. **e** Inner vein selvage: pyrite (py) and chalcopyrite (ccp) replace rutile (rt) lamellae after Ti-magnetite, plane polarized light reflected in air. **f** Outer mottled vein selvage: ophitic igneous texture, ankerite (dark) fills augite sites, and muscovite + quartz replace albite laths, opaque disseminated pyrite, plane polarized light. **g** GMD below the lode: chlorite (chl) pseudomorph after cumulate augite enclosing albite laths. The groundmass consists of chlorite, albite and Fe-calcite (stained blue). Plane polarized light. **h** GMD below the lode: calcite (cal) porphyroblast (stained pale violet) zoned to an iron-rich rim (blue), and albite laths in the chlorite-rich groundmass. Plane polarized light

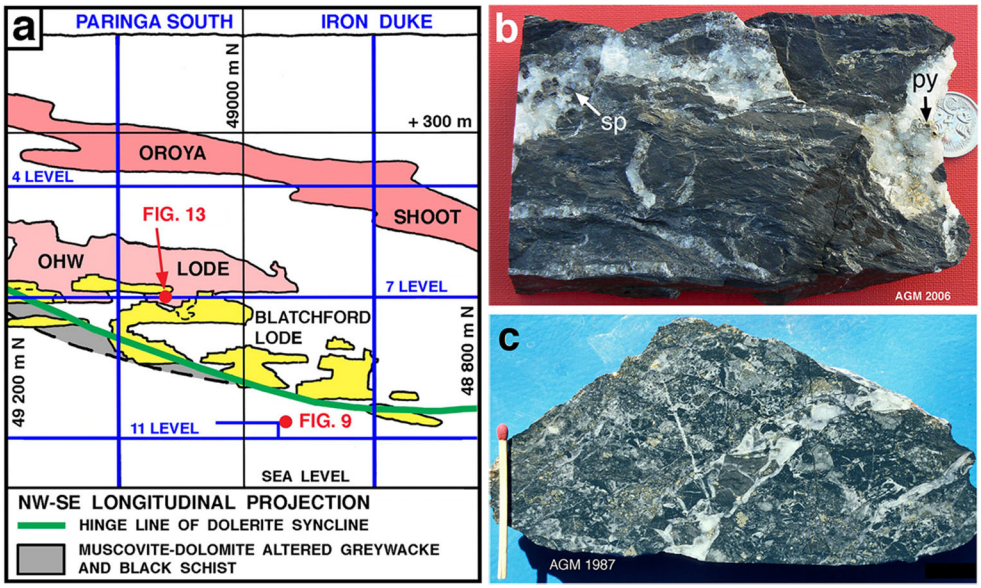

Fig. 8 Structural setting of the D2b Blatchford Lode and the D3a Oroya shear-zone system, Paringa South mine, Golden Mile, Kalgoorlie. **a** Looking northeast at a longitudinal projection of the D1 Brownhill Syncline showing the stopes of the Oroya Shoot, the Oroya Hanging Wall (OHW) Lode, and the Blatchford Lode between the Paringa South and Iron Duke shafts (modified from Tomich 1959). The locations of the lode exposures mapped are shown. The coordinates are mine grid. **b** Oroya 809 ore body, 7 level: Meta-greywacke altered to sericite-quartz-pyrite ± Fe-dolomite schist containing 10 wt.% carbon, crosscut by quartz veins mineralized with sphalerite (sp) and pyrite (py). The coin is 19 mm across. **c** Blatchford 902 breccia ore body, 9 level: fragments of sericite-ankerite altered Paringa Basalt are replaced by Oroya Stage 1 chlorite and pyrite, and cemented by white ankerite, grey quartz, green chlorite, pyrite (5%), and sphalerite (0.5%). The matchstick is 4 cm long

The D2b Blatchford Lode was mapped in muscovite-ankerite altered Paringa Basalt at 48,968 m north and 19,641 m east in the 1109 drive 10 m above the 11 level of the Paringa South shaft (Fig. 8a). At this location, the lode is linked to the adjacent shear zone by a telluride extension vein indicating a syn-mineralization phase of D2c sinistral strike-slip (Mueller 2017, this issue). Strike-slip alternated with reverse movement during D3a shortening, as indicated by the shear-zone S-fabric and by the buckling of the extension vein (Fig. 9). The host rock pillows are slightly flattened in the plane of a cleavage (N60° W/60–75° SW), which is crosscut by both the Blatchford shear zone and the vein (Fig. 9).

Blatchford shear zone

The Blatchford shear zone consists of (1) ductile S-C mylonite 5–12 cm thick (Fig. 10a) marking the main fault surface; (2) fault-fill veins 0.5–2 cm thick forming a parallel hanging wall array (Fig. 9); (3) dark grey pyrite-rich silica-carbonate-chlorite rock (Fig. 10b); and (4) lenses of foliated fault breccia (Fig. 10c) up to 50 cm thick. Three successive alteration and mineralization stages are distinguished: early muscovite-ankerite-quartz characterized by arsenical pyrite ± chalcopyrite (Fimiston-style), intermediate chalcedony-chlorite-siderite characterized by pyrite-pyrrhotite ± arsenopyrite ± sphalerite (Oroya Stage 1), and late quartz-dolomite-calcite veins containing tellurides (Oroya Stage 2). The chlorite temperature estimates of Oroya Stage 1 mineralization are 402 ± 50 °C (Table 1).

Mylonite and fault-fill veins The footwall S-C mylonite varies along strike and down dip from fault-parallel schist enclosing quartz-ankerite boudins and pinch-and-swell veins (Fig. 10a) to wider parts where the C-foliation wraps domains with an oblique S-fabric. Where chlorite and sphalerite are absent, such as 20 m northwest of the face mapped, the mylonite consists of muscovite, ankerite, and quartz (25–30 vol.% each), pyrite (10%), tourmaline (3%), and rutile (Tables 1 and 2). The Fimiston-style pyrite contains inclusions of chalcopyrite and native gold, and is zoned from poikilitic cores (0.82 wt.% As) to solid rims (0.13% As; Fig. 10d). Trace barite is present but albite is absent.

Chlorite and sphalerite indicate the Oroya Stage 1 overprint (Fig. 9). Veins are more abundant (Fig. 10b, e), separated by mm-thick seams of muscovite-quartz-rutile schist, and composed of granular quartz, ankerite, and minor Fe-calcite and tourmaline (0.5–5%). Chlorite and muscovite line the margins. Lithons of wall rock are partly replaced by Fe-chlorite (40%), muscovite (25%), and granular quartz (20%). The sulfide assemblage comprises pyrite, pyrrhotite, chalcopyrite, sphalerite, and arsenopyrite (Table 2). The fault-fill veins in the hanging wall are similar in mineralogy to those in the mylonite.

Silica-carbonate-chlorite replacement Oroya Stage 1 silica-carbonate-chlorite rock forms lens-shaped bodies within the mylonite and along its footwall contact (Fig. 10b) and replaces the inter-pillow material in the wall rock between the shear zone and the telluride vein. Additional replacement by silica,

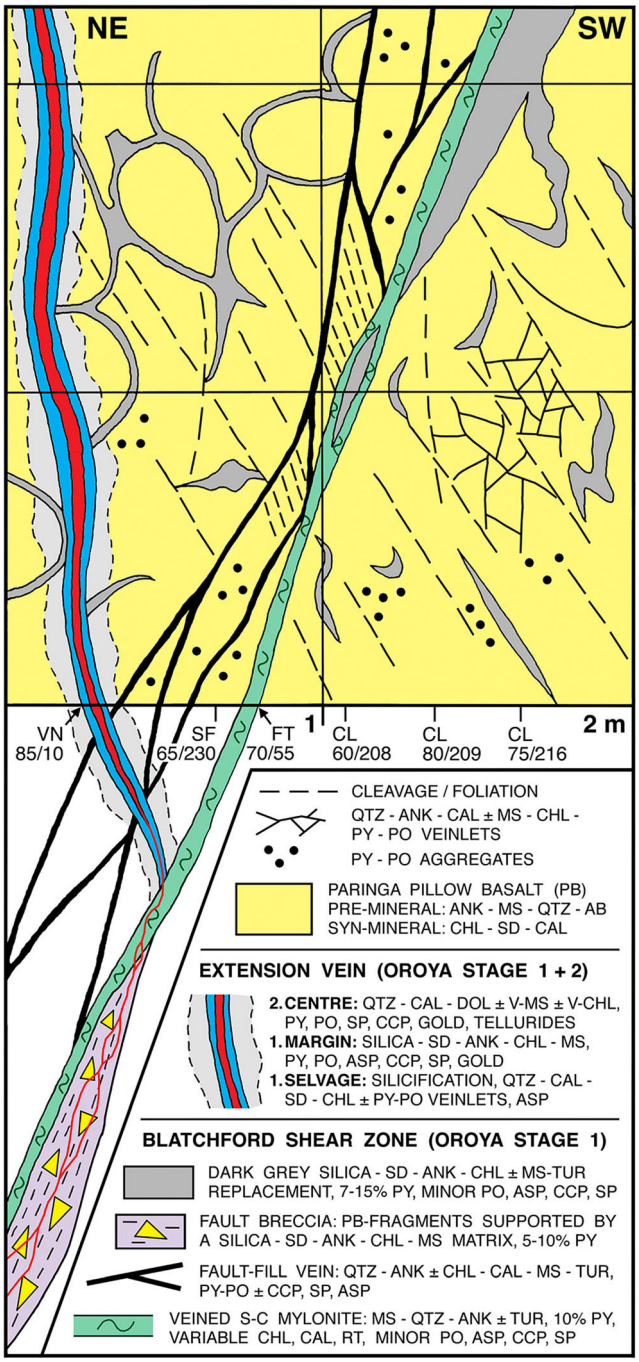

Fig. 9 Northeast-southwest cross section of the D2b Blatchford shear zone and telluride extension vein, 1109 sublevel 10 m above the Paringa South shaft 11 level. The extension vein formed during D2c sinistral strike-slip alternating with reverse oblique-slip during D3 shortening, which generated the S-fabric in the shear zone and caused the buckling of the vein. Late veins (red) crossing breccia in the shear zone are feeders to the extension vein. Structural data are dip angle + dip direction. Structures: cleavage (CL), fault (FT), S-fabric (SF), vein (VN). Minerals: albite (ab), ankerite (ank), arsenopyrite (asp), calcite (cal), chalcopyrite (ccp), chlorite (chl), dolomite (dol), muscovite (ms), quartz (qtz), pyrrhotite (po), pyrite (py), rutile (rt), siderite (sd), sphalerite (sp), tourmaline (tur), vanadian chlorite (V-chl), vanadian muscovite (V-ms)

classified as chalcedony due to its porous nature, also occurs along and between cleavage planes (Fig. 9). The chalcedony encloses siderite-ankerite aggregates (25–30 vol.%), Fe-chlorite (5–10%; Table 1), muscovite (5%), tourmaline (1–3%), and granular rutile (1%) resulting in a finely mottled texture (Fig. 10f). Crackle fractures are lined with the same minerals. Fine-grained pyrite (10–15%) close to the mylonite gives way to an outer pyrite-pyrrhotite assemblage (7–10%) in contact with chalcopyrite, sphalerite and arsenopyrite. Pyrrhotite and the absence of magnetite indicate low oxidation and sulfidation states (Table 2).

Foliated fault breccia Fault breccia exposed in the rise to the 1109 sublevel pinched out below the junction of the telluride vein with the Blatchford shear zone. The breccia matrix supports angular to sub-rounded fragments of Paringa Basalt (Fig. 10c). The fragments are partly replaced by ferroan calcite (10–15 vol.%) but retain most of their pre-sulfide mineralogy (30–40% ankerite, 30% muscovite, 15% quartz). Most contain plagioclase microlites (5 vol.%) pseudomorphed by granular albite and quartz. The breccia matrix consists of Oroya Stage 1 chalcedony (30%), siderite (25%), ankerite (15%), Fe-chlorite (10%), muscovite (7%), rutile (2%), and disseminated pyrite (7%). The texture varies from finely banded to massive. Mineral bands surround micro-fragments of Paringa Basalt and form nodular aggregates zoned from siderite rims to chlorite-muscovite cores (Fig. 10g).

Oroya Stage 2 crackle veins cut across both matrix and fragments. The veins have straight walls, lack selvages, and are filled with quartz (20%) and carbonate (70%) zoned from dolomite cores to ankerite rims (Fig. 10h). Minor muscovite and trace (0.5%) chlorite, sphalerite, and tellurides are present. The low-density vein network represents the up-flow link to the extension vein (Fig. 9).

Telluride extension vein

The extension vein (120 g/t Au) branches off the Blatchford shear zone, widens to 10 cm in the face mapped, and is gently buckled down dip (Fig. 9). In July 1987, the vein had been stoped 25 m to the east of the 1109 sublevel. It has sharp walls and is zoned from Oroya Stage 1 chalcedony-sulfide margins to central Stage 2 quartz-carbonate-telluride fill (Fig. 11a). A bulk XRD sample indicates that quartz, calcite, and ferroan dolomite are major, whereas pyrite, siderite, and phengitic muscovite are minor (Table 1). The Fe^{3+}/Fe^{2+} ratio, presence of pyrrhotite, and absence of magnetite suggest a low oxidation state (Table 2).

Oroya Stage 2 quartz-carbonate fill The central light grey part of the vein consists of strained quartz crystals pointing inward (30 vol.%; 1–5 mm). Most are rimmed by recrystallized

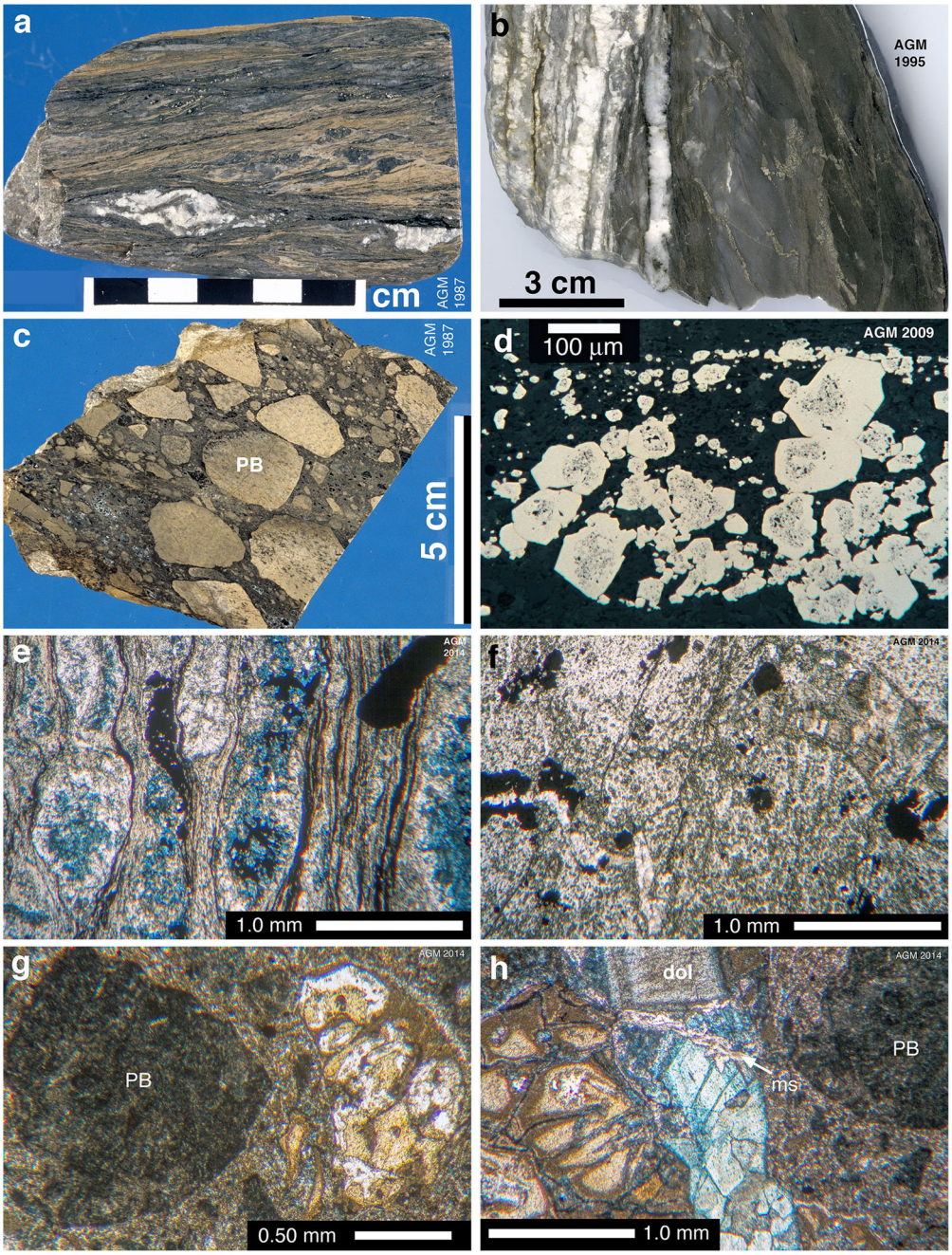

Fig. 10 Textures and mineral assemblages in the D2b Blatchford shear zone, 1109 sublevel, Paringa South shaft 11 level. The host rock is sericite-ankerite altered Paringa pillow basalt. **a** Fimiston ore: Muscovite-ankerite-quartz S-C mylonite, white-grey ankerite-quartz boudins, 10 vol.% arsenical pyrite, black tourmaline. 1109 sublevel, 20 m NW of the face mapped. **b** Oroya Stage 1: mylonite (left) marked by quartz-ankerite ± chlorite ± muscovite veins and seams of muscovite-quartz-pyrite schist. The dark silica replacement (right) consists of 50% chalcedony, 25% ankerite, 10–15% pyrite, 10% chlorite and muscovite, and 1–3% tourmaline and rutile. 1109 sublevel. **c** Oroya Stage 1: fault breccia, fragments of sericite-ankerite altered Paringa Basalt (PB) cemented by a chalcedony-siderite-ankerite matrix containing Fe-chlorite (10%), muscovite (7%), rutile (2%), and pyrite (7%). 11 level rise to the 1109 sublevel. **d** Fimiston ore: arsenical pyrite in the S-C mylonite (**a**) zoned from poikilitic cores to solid rims, micron-sized grains of native gold are at the core-rim boundary, plane polarized light reflected in air. **e** Oroya Stage 1: pinch-and-swell veins in mylonite composed of quartz + ankerite ± Fe-calcite (both stained blue) in muscovite-quartz-rutile schist, opaque pyrite-pyrrhotite aggregates, plane polarized light. **f** Oroya Stage 1: replacement of porous chalcedony (white) mottled by ankerite-siderite-chlorite aggregates. Muscovite, rutile and carbonate line fractures, pyrite-pyrrhotite ± chalcopyrite ± sphalerite ± arsenopyrite aggregates are opaque, plane polarized light. **g** Oroya Stage 1: fault breccia, siderite-silica-pyrite matrix supporting fragments of sericite-ankerite altered Paringa Basalt (PB; stained dark blue). The nodular aggregate consists of brown siderite ± rutile, yellow Fe-chlorite, and white muscovite + quartz, plane polarized light. **h** Oroya Stages 1 and 2: fault breccia crosscut by a Stage 2 vein of dolomite (dol), ankerite (stained light blue), and muscovite (ms) ± quartz. The zoned aggregates of siderite, Fe-chlorite, and muscovite + quartz are Stage 1 matrix supporting fragments of Paringa Basalt (PB), plane polarized light

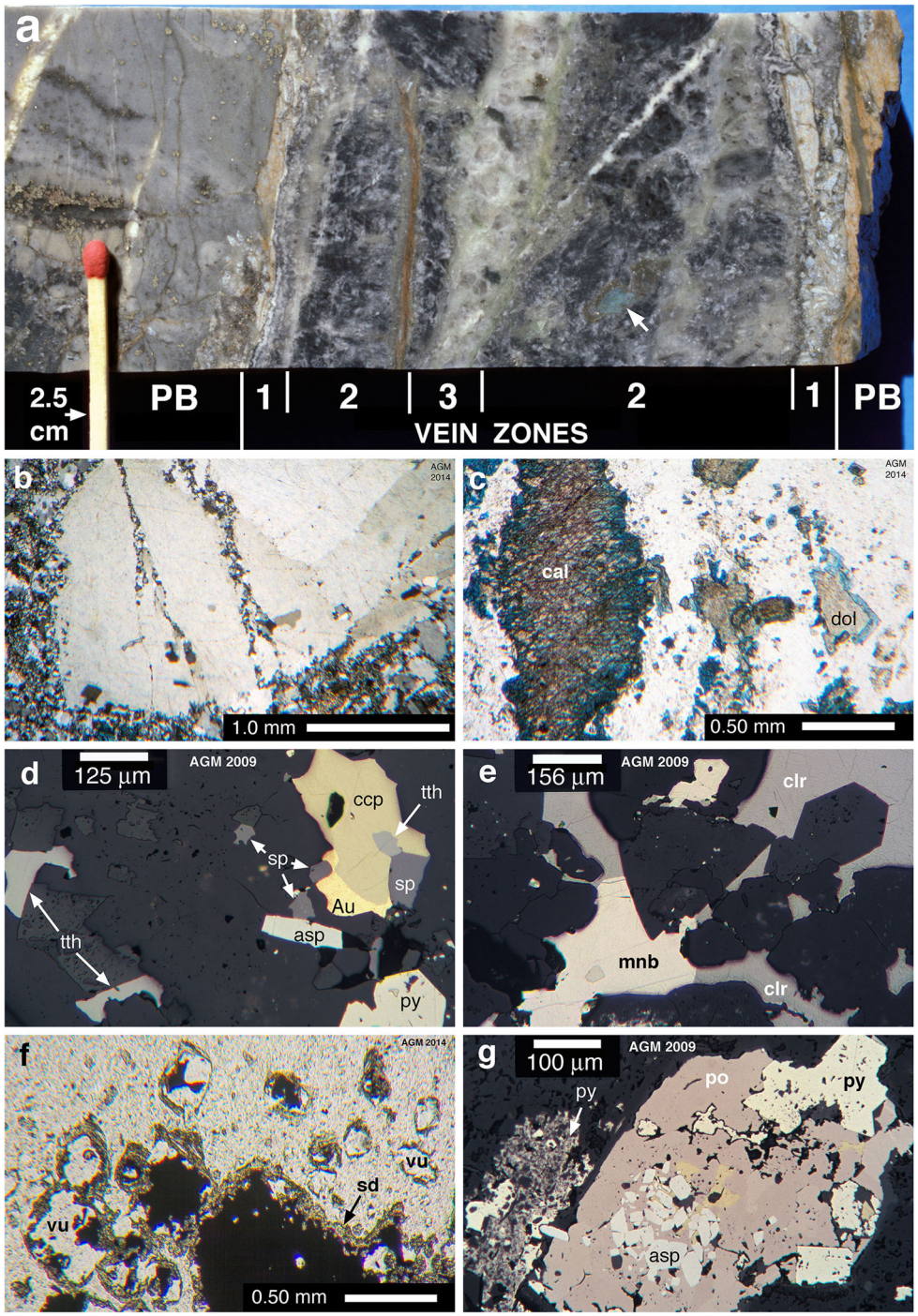

Fig. 11 Textures and mineral assemblages in the extension vein (Oroya Stages 1 and 2) branching off the D2b Blatchford shear zone, 1109 sublevel, Paringa South shaft 11 level. **a** Section through the zoned vein in fractured and silicified Paringa Basalt (PB). Zone 1: Stage 1 chalcedony fill and replacement, minor muscovite, ankerite, siderite, and chlorite, and pyrite + pyrrhotite ± arsenopyrite ± sphalerite; zone 2: Stage 2 columnar black calcite and grey quartz crystals, in part comb-textured, interstitial granular quartz and dolomite, V-muscovite (arrow), pyrite + gold + tellurides; zone 3: Stage 2 comb-textured quartz crystals, interstitial granular quartz, minor dolomite and calcite, V-muscovite, pyrite + gold + tellurides. **b** Stage 2: pointed quartz crystal crossed by healed fractures in a matrix of granular quartz and minor calcite, vein zone 3, crossed polarized light. **c** Stage 2: calcite (cal; stained red brown) zoned to ferroan rims (dark blue), and dolomite (dol) zoned to ankerite rims (light blue) in a matrix of granular quartz, vein zone 2, plane polarized light. **d** Stage 2: assemblage chalcopyrite (ccp) + sphalerite (sp) + tetrahedrite (tth) + gold (Au) adjacent to pyrite (py) and arsenopyrite (asp), vein zone 2, plane polarized light reflected in air. **e** Stage 2: coloradoite (clr) in contact with montbrayite (mnb), vein zone 2, plane polarized light reflected in air. **f** Stage 1: opaque sulfide aggregates rimmed by siderite (sd) in a matrix of chalcedony containing disseminated muscovite and open vughs (vu), vein zone 1, plane polarized light. **g** Stage 1: pyrrhotite (po) enclosing arsenopyrite (asp) and chalcopyrite (yellow) in contact with pyrite (py), and an aggregate of dendritic pyrite (left) in chalcedony, vein zone 1, plane polarized light reflected in air

margins, and some are crossed by healed fractures (Fig. 11b). The comb texture indicates open-space filling. The matrix consists of microcrystalline granular quartz (40–45%), dolomite zoned to ankerite rims (10%), and calcite zoned to ferroan rims (10%). Green muscovite (5%), red chlorite (0.5%), and rutile form stylolite seams and are enriched in vanadium (Tables 1 and 2).

The quartz-rich central part is zoned symmetrically to black-grey outer fill (Fig. 11a) composed of ferroan calcite (50–70 vol.%), minor quartz (20%), dolomite (5–15%), V-muscovite (5%), and Fe-V chlorite, rutile, and apatite (all 0.5%). The calcite is zoned to iron-rich rims and the dolomite to outer ankerite (Fig. 11c). Strained columnar calcite (5 mm) and pointed quartz crystals (1.5 mm) oriented at a high angle to the walls indicate that this part of the vein also formed by open-space filling. Like in the center, the matrix between the columnar crystals is composed of microcrystalline quartz and carbonate.

The sulfide assemblage comprises subhedral pyrite (3%), minor chalcopyrite, sphalerite and tetrahedrite, and rare bornite-covellite-digenite aggregates indicating a late trend to higher sulfur fugacity (Table 2). The sulfides are in contact and in spatial association with native gold and tellurides (Fig. 11d, e) including coloradoite (HgTe), montbrayite ($[Au,Sb]_2[Te,Sb]_3$), tellurantimony (Sb_2Te_3), antimonian calaverite ($[Au,Sb]Te_2$), altaite (PbTe), and petzite (Ag_3AuTe_2). Melonite ($NiTe_2$), pyrrhotite, and arsenopyrite are present close to the chalcedony margin of the vein fill.

Oroya Stage 1 chalcedony fill The blue-grey zones at both walls of the vein (Fig. 11a) consist of granular and lesser fibrous chalcedony (40–50 vol.%), ankerite (10–30%), siderite (5%), muscovite (20%), chlorite (1–2%), rutile (2%), and accessory tourmaline and apatite (both 0.5%). The chalcedony matrix has open vughs (Fig. 11f) and is finely banded in nodular aggregates of ankerite, siderite-sulfide, and muscovite-chlorite. Seams of granular to needle-shaped rutile, in particular at the wall-rock contact, suggest some replacement during the initial opening of the vein. Pyrite (5–10%) forms subhedral crystals and atoll-shaped or dendritic aggregates (Fig. 11g) in contact with pyrrhotite (1–3%) and arsenopyrite, the assemblage indicating a low sulfidation state (Table 2). Minor chalcopyrite and sphalerite, and trace native gold and melonite are associated.

Outer mineralization in Paringa Basalt

Light blue-grey silica selvages extend from the telluride vein 3–10 cm into the wall rock fading outward and merging with the dark grey silica replacement lining the pillows (Fig. 9). Veinlets crossing the selvage control some of the replacement. They are filled with chalcedony and calcite, and with accessory ankerite, siderite, muscovite, and chlorite. Quartz replaces the plagioclase microlites. Rutile (2–10 μm) is more abundant (3 vol.%) in the selvage than in the extension vein. Sulfides line fractures and pyrite-pyrrhotite aggregates (2%), arsenopyrite (2%), and tourmaline (0.3%) are disseminated.

A channel sample cut across the Paringa Basalt between the vein and the Blatchford shear zone assayed 1.85 g/t gold. A bulk sample of least-altered wall rock contained 0.46 g/t gold, the grade attributed to low intensity silica-chlorite alteration and sulfide mineralization controlled by SW-dipping cleavage planes and by crackle veinlets (Fig. 9). The veinlets are filled with quartz, dolomite-ankerite, ferroan calcite, minor muscovite, and Fe-chlorite. Pyrite-pyrrhotite aggregates are in contact with accessory sphalerite, chalcopyrite, arsenopyrite, and ullmannite (NiSbS).

The Oroya Hanging Wall Lode

The Oroya Hanging Wall (OHW) Lode is located in the main reverse fault controlling the telluride-rich Oroya Shoot (115 g/t Au; Simpson 1912), the type locality of Oroya-style mineralization. Both form major ore bodies above level 7 of the Paringa South shaft (Fig. 8a). The D3a OHW shear zone follows the GMD-PB contact at the SW-limb of the Kalgoorlie Anticline and displaces D2a and D2b faults 50 m SW-side up (Mueller 2017, this issue). The strike varies from N25° W to N35° W, and the dip from 35° to 60° SW. The lode was mapped on the Paringa South shaft 7 level (162 m above sea level) at 49,070 m north and 19,792 m east, where the main crosscut meets the OHW drive.

In the crosscut and in pillars of the adjacent stope, the lode replaces sericite-ankerite altered Paringa pillow basalt (Fig. 12a). It consists of siliceous S-C mylonite and fault breccia formed by Oroya Stage 1 silica-chlorite-siderite ore rich in pyrite, and by Stage 2 silica-ankerite ore containing native gold and tellurides. Chlorite temperature estimates are 415–425 °C for Stage 1, and 385 °C for Stage 2 (Table 1). Fimiston-style mineralization is absent. Opposite the crosscut, the stope extends up to 4 m below the lode due to a network of crackle veinlets, silica-sulfide replacement, and extension veins. The veins strike perpendicular to the lode and are characterized by comb-textured quartz (Fig. 12b). Adjacent light brown basalt is replaced by dark green chlorite and siderite.

Internal structure of the OHW Lode

On the Paringa South shaft 7 level, the OHW Lode (48 g/t Au) is 1.5–2.0 m thick and characterized by Stage 1 chert-like silica, probably chalcedony recrystallized during shear movement. The uppermost part consists of black mylonite containing intrafolial veins (Fig. 12c) derived from carbonaceous greywacke trapped below the GMD sill. The black mylonite

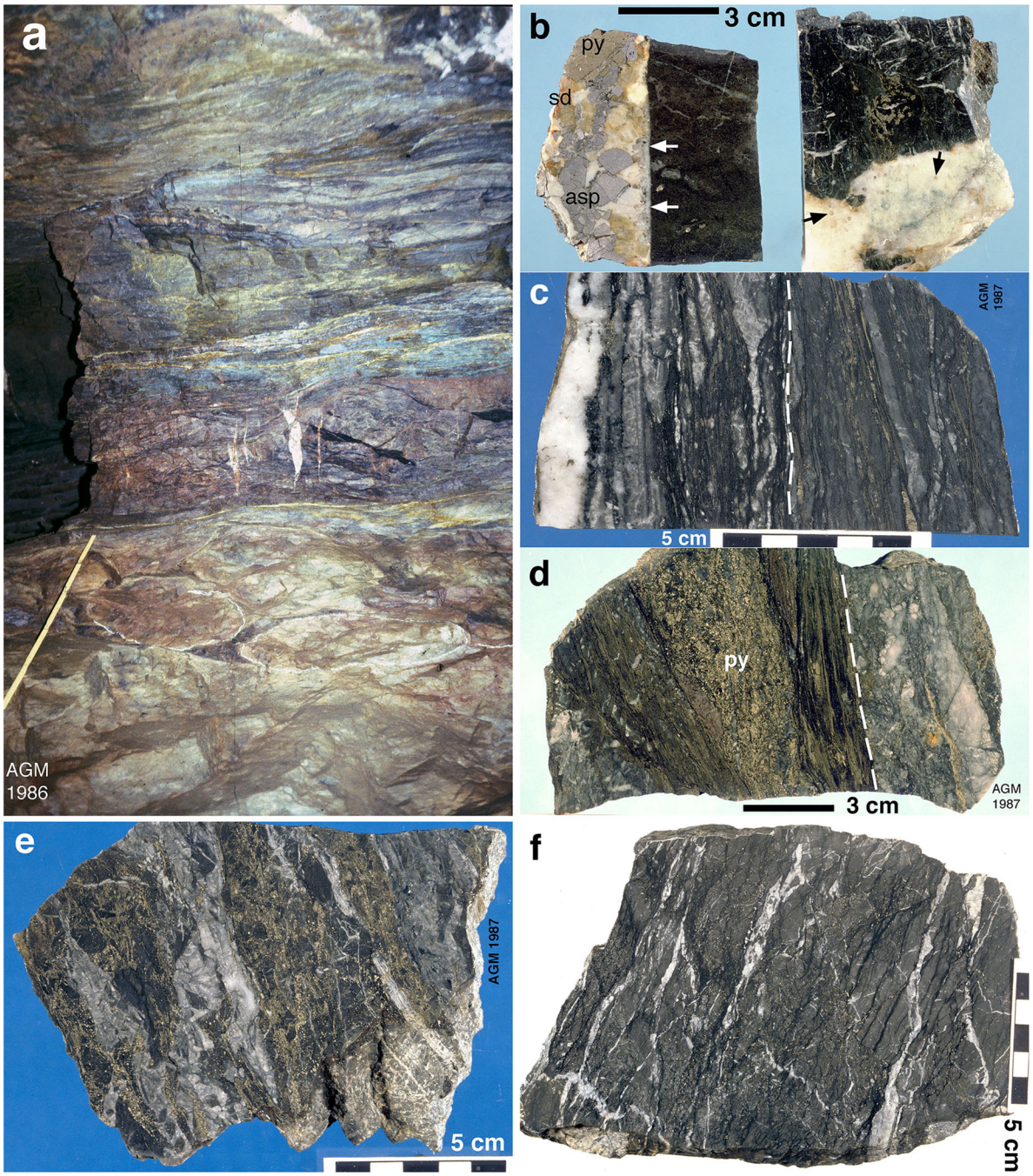

Fig. 12 Structures and textures in the D3a Oroya Hanging Wall (OHW) Lode, Paringa South shaft 7 level. Ore pillar and Stage 3 veins in the stope northeast of the OHW drive **(a**, **b)**, and samples of Oroya Stage 1 and Stage 2 ore **(c**–**f)** from the exposure mapped (Fig. 13) in the crosscut. **a** Looking N50° E at a stope pillar (49,000 m N, 19785 m E). The lode is composed of rusted, pyrite-rich siliceous mylonite and micro-brecciated silica-chlorite-siderite rock. Thin muscovite-chlorite-quartz S-C mylonite separates the lode from sericite-ankerite altered Paringa Basalt below. Pillows are outlined by chalk, the yellow scale is 100 cm. **b** Extension veins (Stage 3): euhedral quartz crystals indicating open-space filling line the walls (white arrows), and display six-sided sections within veins (black arrows). Many veins contain ankerite, siderite (sd), pyrite (py), arsenopyrite (asp), sphalerite, and native gold. The sericite-ankerite assemblage in Paringa Basalt is replaced by chlorite + siderite + pyrite. **c** Upper siliceous mylonite (Stage 1): contact (broken line) between black siliceous mylonite (left; 2 vol.% organic matter) marked by quartz-ankerite veins, and dark grey tourmaline-bearing siliceous mylonite (right; no organic matter), both mineralized with pyrite (15%) and arsenopyrite (1%). **d** Siliceous mylonite (Stage 1 + 2): Contact (broken line) between dark grey siliceous mylonite (left) enclosing a lens of massive pyrite (py)-siderite-ankerite-chlorite rock (Stage 1), and banded white-grey silica-ankerite fill (right; Stage 2) mineralized with pyrite, native gold, and tellurides. **e** Breccia (Stage 1 + 2): fragments of dark grey, pyrite-rich silica-chlorite-siderite ore (Stage 1) cemented by white-grey silica and ankerite (Stage 2) containing pyrite, gold and tellurides. **f** Silica-chlorite-siderite rock (Stage 1 + 2): dark grey chert-like silica containing disseminated pyrite + muscovite, crossed by black chlorite-siderite-pyrite seams, grades into micro-breccia cemented by chlorite and siderite (Stage 1). White ankerite-quartz veins (Stage 2) crosscut the other structures

grades downward into dark grey siliceous mylonite enclosing lenses of semi-massive pyrite (Fig. 12d), which is in discordant contact with a light grey brecciated zone of Stage 2 silica-ankerite fill cementing fragments of the dark silica (Fig. 12d, e). The central part of the lode consists of fractured and microbrecciated silica-chlorite-siderite rock (Fig. 12f), and of silica-mottled siderite-ankerite-chlorite rock representing less intense silicification. XRD of a bulk sample indicates that quartz, ankerite and chlorite are abundant, siderite and pyrite are minor, muscovite is rare, and albite below detection. The whole-rock Fe^{3+}/Fe^{2+} ratio is low (Table 2).

Oroya mineralization in GMD

In Golden Mile Dolerite, economic Oroya Stage 1 mineralization is confined to the 1–2 cm thick muscovite-chlorite-quartz S-C mylonite lining the hanging wall of the lode (Fig. 13). Albite, calcite, siderite, and deformed rutile trellis (0.4 mm) are minor. Pyrite (10 vol.%) is in contact with chalcopyrite and gersdorffite and encloses grains of muscovite, rutile, pyrrhotite, and melonite (5–15 μm).

The S-C mylonite grades upward into a parallel zone 20–30 cm thick of foliated GMD Unit 1 (20–40% muscovite, 5–20% chlorite, 30–50% granular quartz + albite). Pinch-and-swell ankerite-pyrite veins are rimmed by muscovite, quartz and chlorite. The veins are linked by ladder veinlets of similar composition. Seams of rutile, quartz, and pyrite trace the foliation. Primary textures are not preserved except for interstitial igneous quartz (1%) and trellised rutile lamellae after Ti-magnetite.

The GMD Unit 1 above is cut by spaced cleavage planes sub-parallel to the OHW Lode but retains some of its variolitic texture. Ankerite, ferroan calcite, quartz, and minor muscovite and chlorite fill crackle veinlets. Both carbonates also form part of the wall rock (20–30% in total). Muscovite is the only white mica present (35 vol.%; SWIR absorption at 2194.7 nm), at least up to the narrow D2a lode of the Federal system composed of muscovite, ankerite and pyrite (Fig. 13).

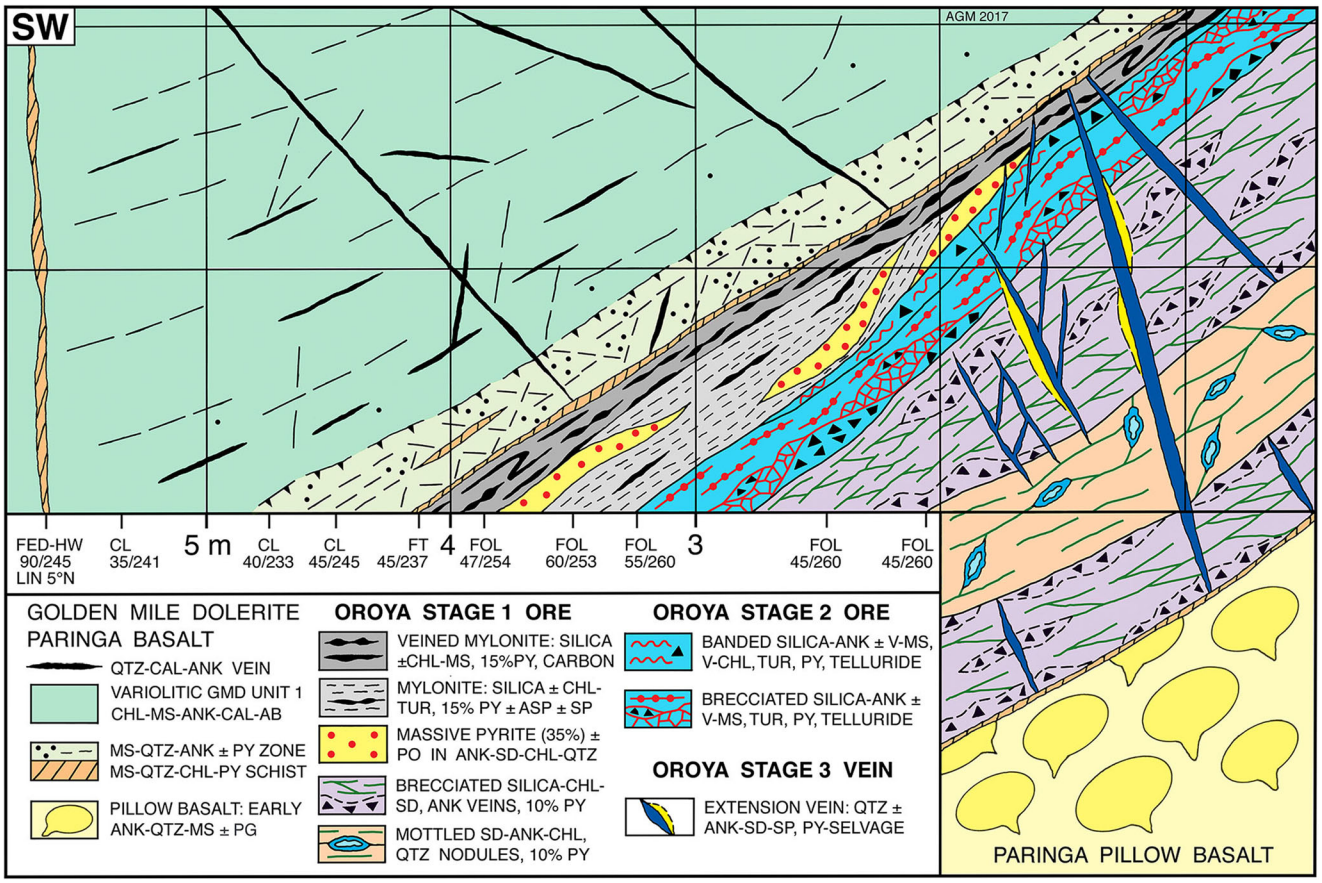

Fig. 13 Northeast-southwest cross section through the D3a Oroya Hanging Wall (OHW) Lode, main crosscut at the intersection with the OHW drive, Paringa South shaft 7 level. The lode (48 g/t Au) offsets a D2a Fimiston Lode of the Federal system (FED-HW) and follows the contact of the Golden Mile Dolerite (GMD) sill. Chert-like silica replaces 15 cm thick carbonaceous greywacke and the Paringa Basalt below, both rocks altered to a sericite-ankerite assemblage prior to Oroya-style mineralization. Stage 2 pyrite-telluride ore crosscuts Stage 1 pyrite-arsenopyrite ore. Structural data are dip angle + dip direction. Structures: cleavage (CL), foliation (FOL), fault (FT), lineation (LIN). Minerals: albite (ab), ankerite (ank), arsenopyrite (asp), calcite (cal), chlorite (chl), muscovite (ms), quartz (qtz), paragonite (pg), pyrrhotite (po), pyrite (py), siderite (sd), sphalerite (sp), tourmaline (tur), vanadian chlorite (V-chl), vanadian muscovite (V-ms)

Oroya Stage 1 pyrite ore

Below the GMD contact, disseminated pyrite averages 15 vol.% in the upper siliceous mylonite. Intercalated sulfide lenses contain up to 35% pyrite cemented by ankerite, siderite, quartz, and chlorite. Below the crosscutting telluride zone (Fig. 13), the pyrite content is more variable (7–15%) and post-kinematic cubes and aggregates (3–10 mm) are common. Stage 1 pyrite is intergrown with minor arsenopyrite, sphalerite and chalcopyrite and encloses rare grains of anhedral pyrrhotite indicating a low to intermediate sulfidation state (Table 2). Micron-sized grains of native gold, melonite, and coloradoite are in contact with or enclosed in both pyrite and arsenopyrite (Fig. 14a).

Siliceous mylonite The mylonite consists predominantly of silica (40–60 vol.%) laminated by surfaces lined with Fe-Mg chlorite (7–10%; Table 1), muscovite (2%), and rutile (0.2–0.5%). The upper part is black due to amorphous organic matter (1–2%) and marked by pinch-and-swell or drag-folded veins composed of granular quartz, ankerite, and sulfides. Ankerite (15%), siderite (2%), tourmaline (1–10%), and the sulfides are also concentrated in seams parallel to foliation (Fig. 14b). The tourmaline changes from blue-grey to yellow-red towards the telluride zone but is the only mineral enriched in V_2O_3 (0.2–0.4 wt.%).

Brecciated silica-chlorite-siderite rock Silica-chlorite-siderite replacement, separated from the upper mylonite by the zone of late-stage telluride ore, forms the central and footwall parts of the lode (Fig. 13). Dark grey silica enclosing micron-sized pyrite (3–5 vol.%), muscovite (1–5%), tourmaline, and apatite (0.2%) alternates with lenses of micro-breccia (0.1–5 mm fragments). A network of fractures roughly parallel to the lode boundaries crosscuts the grey silica (Figs. 12f and 14c). The fractures are lined with mm-thick seams of Fe-chlorite, pyrite, and accessory siderite, rutile, and arsenopyrite. Most chlorite seams terminate at micro-breccia, which consists of embayed fragments of dark grey silica (Fig. 14d) supported by a matrix of Fe-chlorite (35–50%), siderite (15–50%), quartz (5–15%), and rutile (1%). Chlorite-rutile stylolites cross the matrix locally.

Silica-mottled siderite-ankerite-chlorite rock Light grey carbonate-rich ore is located between the micro-brecciated siliceous zones (Fig. 13). A mottled texture is imparted by aggregates (0.5 mm) of microcrystalline quartz (15–30 vol.%) located within broader domains of siderite (15–25%), Fe-Mg chlorite (5–15%), and ankerite. Stylolite seams of Fe-Mg chlorite, rutile, and muscovite define a spaced foliation sub-parallel to the lode walls. Chlorites in the silica-mottled rock and in the siliceous mylonite are more Mg-rich ($Mg / [Mg + Fe^{2+}] = 0.4–0.5$) than those in brecciated silica ($Mg / [Mg + Fe^{2+}] = 0.2–0.3$) but all are low in vanadium (0.1–0.2 wt.% V_2O_3; Table 1).

Oroya Stage 2 pyrite-telluride ore

The discordant zone of Stage 2 pyrite-telluride ore is subdivided into an upper banded and a lower brecciated part. The upper bands are 2–10 mm thick and composed of fractured light grey silica (25–45 vol.%) and white sparry ankerite (30–65%), some grains enclosing dolomite cores. The ankerite bands contain sparse fragments (1–5 mm) of Stage 1 silica, characterized by micron-sized pyrite and muscovite, and fragments of pure silica derived from intercalated bands. The ankerite is intergrown with siderite (1–3%), red Fe-V chlorite (0.5–2%), and rare fluor-apatite. The bands are separated by seams of red tourmaline (Fig. 14e) and by stylolites of green V-muscovite, both in contact with pyrite (3–5% in total) and accessory rutile, Fe-chlorite and Fe-V chlorite (Table 1).

The lower part of the telluride zone consists of crackle breccia, jig-saw breccia (Fig. 14f), and matrix-supported breccia. The white-grey silica-ankerite matrix (40 vol.%) described above cements fragments (0.5–2 cm) of dark grey siliceous mylonite and of silica-siderite-chlorite rock (about 60 vol.% in total). The cement contains seams and stylolites of vanadian tourmaline, chlorite, and muscovite. Pyrite (3–5%) and associated chalcopyrite, sphalerite, native gold, montbrayite, antimonian calaverite, tellurantimony, coloradoite, and altaite (Fig. 14g; Table 2) are disseminated and concentrated along stylolite surfaces.

The telluride-bearing breccia grades downward into a network of white veins (5–10 vol.%), which crosscuts the Stage 1 silica-chlorite-siderite ore (Fig. 12f). The veins contain fragments of dark grey silica and are composed of ankerite (70–90%), zoned dolomite-ankerite (1–3%), quartz (10–20%), and accessory muscovite, chlorite, pyrite, sphalerite, and native gold (0.1–1% each). Adjacent aggregates of ankerite or ankerite-muscovite partly replace the earlier chlorite-siderite assemblage (Fig. 14d). Some veins are offset at chlorite-lined surfaces but others cut across.

The vein network is linked to concentrically zoned, nodular veins in the silica-mottled siderite-ankerite ore (Fig. 13). These veins have margins of sparry ankerite or microcrystalline quartz-ankerite and cores of granular or columnar quartz. Locally, they contain small fragments of dark grey silica and aggregates of pyrite (0.5 vol.%). The textures suggest some open-space fill, perhaps in leached cavities. Part of the post-kinematic pyrite disseminated adjacent to veins is attributed to Stage 2, as are covellite-digenite rims on chalcopyrite (Fig. 14h) indicating an increase in sulfur fugacity with time (Table 2).

Oroya Stage 3 extension veins

Extension veins characterized by open vughs link late movement surfaces and crosscut all other mineralized structures (Fig. 13). They consist of coarse-grained (5–10 mm) subhedral to euhedral quartz, ankerite, siderite, pyrite,

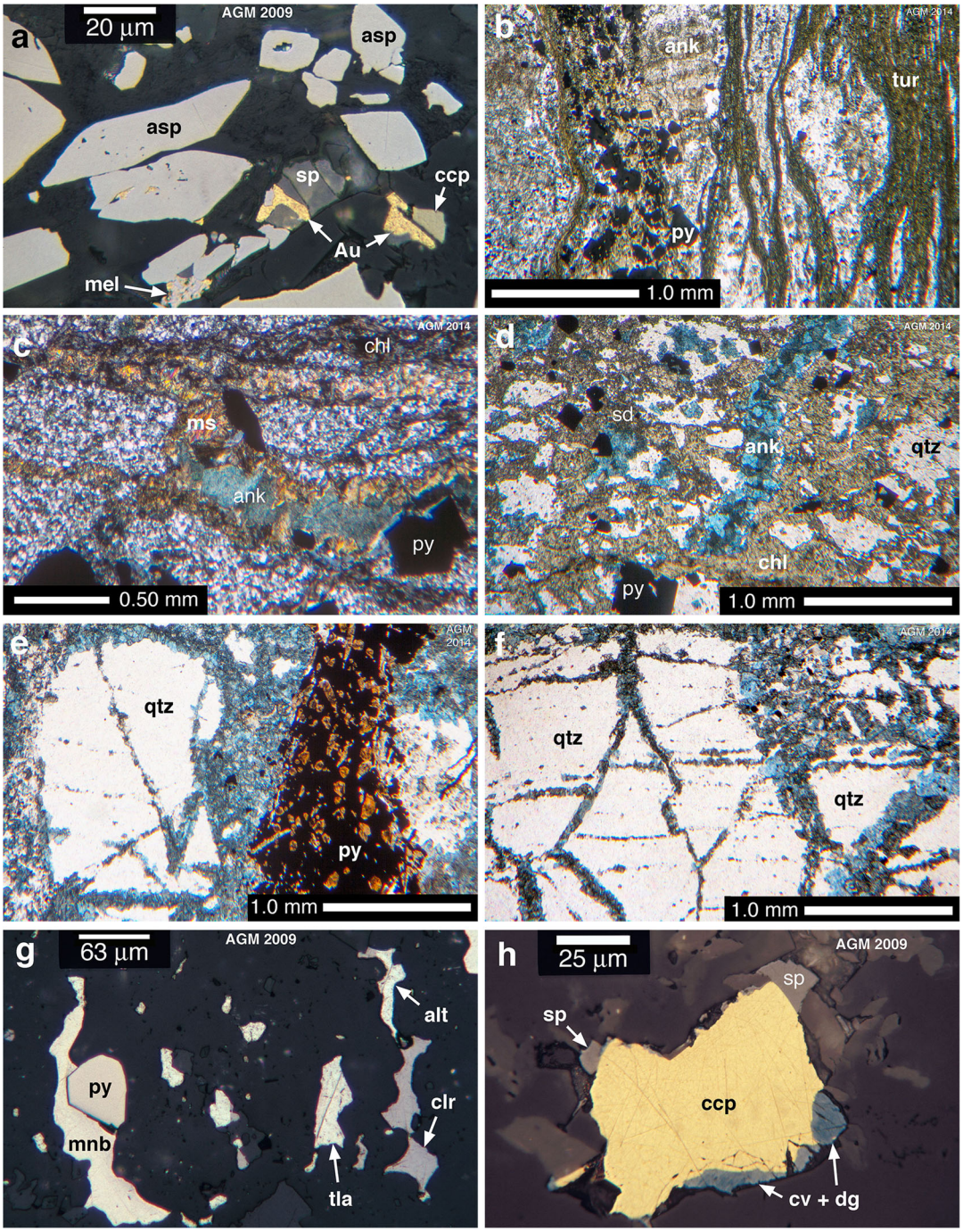

Fig. 14 Minerals and textures in Oroya Stage 1 and Stage 2 ore from the D3a Oroya Hanging Wall Lode (Fig. 13), Paringa South shaft 7 level. **a** Siliceous mylonite (Stage 1): native gold (Au) in contact with sphalerite (sp), chalcopyrite (ccp) and arsenopyrite (asp). The arsenopyrite encloses micron-sized gold, and is in contact with melonite (mel), plane polarized light reflected in air. **b** Siliceous mylonite (Stage 1): domains of chert-like quartz wrapped by fibrous tourmaline (tur) and a band of ankerite (ank) + pyrite (py), plane polarized light. **c** Silica-chlorite-siderite rock (Stage 1): fractured chert-like quartz is crossed by chlorite seams (chl) partly replaced by Stage 2 ankerite (ank, stained blue), muscovite (ms) and pyrite (py), crossed polarized light. **d** Silica-chlorite-siderite rock (Stage 1): micro-breccia, embayed fragments of chert-like quartz (qtz) cemented by chlorite (chl) and siderite (sd), and replaced by Stage 2 ankerite (ank, stained blue) and pyrite (py), plane polarized light. **e** Banded silica (Stage 2): band of opaque pyrite (py) and red vanadian tourmaline in ankerite (stained blue) cementing fractured chert-like quartz (qtz), plane polarized light. **f** Brecciated silica (Stage 2): jig-saw breccia, fragments of chert-like quartz (qtz) are cemented by ankerite (stained blue) and pyrite (opaque), plane polarized light. **g** Brecciated silica (Stage 2): pyrite (py) in contact with montbrayite (mnb) adjacent to coloradoite (clr), altaite (alt) and tellurantimony (tla), plane polarized light reflected in air. **h** Silica-mottled carbonate-chlorite rock (Stage 1): early sphalerite (sp) and chalcopyrite (ccp) rimmed by Stage 2 covellite and digenite (cv + dg), plane polarized light reflected in air

arsenopyrite, and sphalerite (up to 10 vol.% each). The sphalerite is yellow and iron-poor. Native gold (0.5–2 mm) and fan- to rosette-shaped aggregates of Fe-chlorite are accessory (0.5%). Discontinuous replacement selvages of pyrite border some of the veins.

North Kalgurli Flat Lode

The OHW Lode is reduced but Oroya Stage 1 mineralization elsewhere is oxidized, for example in the Flat Lode stoped between the North Kalgurli shaft 13 and 14 levels. The stope (49,140 m N, 19350 m E) is located close to the GMD-PB contact 105 m below sea level. The Flat Lode is 0.6 to 1.2 m thick and controlled by a D3a reverse fault oriented N60–80° W/20–25° SW, which displaces the D2a Lake View Lode (N50° W/70° SW) hanging wall block northeast (Fig. 15a). The D3a lode (5 g/t Au) is composed of red breccia and replacement ore (Fig. 15b).

Oroya Stage 1 breccia ore

The main part of the ore body is clast-supported red breccia. The fragments (2–50 mm) consist of porous, microcrystalline siderite zoned to ankerite rims. Rutile is accessory (0.5 vol.%) and primary textures are absent (Fig. 15c). The fragments are cemented by a coarser-grained matrix of granular or comb-textured siderite and ankerite zoned to inner Fe-chlorite and quartz (Fig. 15d). The chlorite temperature of the breccia cement is 384 ± 50 °C (Table 1). Most fragments are partly replaced by chlorite and by microcrystalline silica, and both fragments and matrix contain disseminated oxide-sulfide aggregates composed of magnetite (0.21 wt.% V_2O_3), hematite (0.40–0.75% V_2O_3; ≤ 2.9% TiO_2), pyrite, and chalcopyrite. Contact relations indicate a high oxidation and intermediate sulfidation state (Table 2). Hematite replaces magnetite (Fig. 15e), rims magnetite-pyrite grain boundaries, and fills fractures in pyrite (Fig. 15f). The pyrite is zoned from solid arsenic-poor cores to poikilitic rims enriched in arsenic (Fig. 15f). Micron-sized grains of native gold and hematite are enclosed in or attached to pyrite rims.

Where the stope terminates on level 13, the Flat Lode is composed of a 10-cm-thick mylonite and a 50-cm-thick red replacement zone in green chlorite-calcite altered GMD Unit 5 characterized by trellised rutile lamellae after Ti-magnetite (2–3 vol.%). Thin quartz-ankerite ± albite ± pyrite veins trace the mylonite fabric. The replacement zone is fractured but igneous textures are preserved (Fig. 15b). Interstitial quartz (5%) encloses lath-shaped albite (0.5–1 mm) partly replaced by sericite + ankerite ± hematite. Ankerite and magnetite fill augite sites. Pyrite and magnetite (1–3% each) are in contact.

Mass-balance calculations

The geochemical data in Table 3 are used for mass-balance calculations after the method of Grant (1986) to constrain element enrichment and depletion in gold ore relative to outer chlorite-calcite altered Golden Mile Dolerite or sericite-ankerite altered Paringa Basalt. Aluminium, titanium, phosphorus, and zirconium are chosen as least-mobile elements based on Al/Ti, Ti/P, and Ti/Zr ratios (Table 3). The data and mass balances of samples from the paragonite-ankerite-chloritoid zone of the Trafalgar Fault (App. 2b and 3), and the rare earth element data (App. 2a) and chondrite-normalized REE-patterns (App. 4 and 5) of all samples are presented and discussed in the Electronic Supplementary Material.

Fimiston-style refractory ore

Fimiston-style ore is represented by the Kelly Lode in the Paringa South mine and by the average ore (210,410 t) mined from the Lake View and Perseverance shafts in the Eastern Lode System (Fig. 2a). The pyrite ore of the Kelly Lode lacks iron oxides and has a low Fe^{3+}/Fe^{2+} ratio (0.08; Table 3). The sample is composed of vein replacement selvages in GMD Unit 2. A slight increase in volume caused by veinlets shifts the Ti-P isocon to the right of the equal-mass diagonal line (Fig. 16a). Sulfur, K_2O, and CO_2 are strongly enriched, and silica, Na_2O, CaO, and MnO are moderately enriched, whereas H_2O is depleted (Fig. 16a). These changes reflect the abundance of Fe-Mn dolomite, quartz and albite, and lesser pyrite and phengitic muscovite in the selvages, whereas the loss of H_2O reflects the destruction of chlorite. The trace elements are subdivided into lithophile (Fig. 16b) and chalcophile-siderophile (Fig. 16c). Enrichment is attributed to substitution in muscovite (Ba, Rb, Cs), dolomite (Sr), pyrite (As, Sb, Tl), and chalcopyrite (Cu, Sn). Telluride inclusions in pyrite account for Te, Se, Au, Ag, Hg, and Pb, and scheelite may account for W and Mo. In contrast, lithium and zinc are enriched in chloritic GMD below the lode.

The Fimiston mill-head sample has a high Fe^{3+}/Fe^{2+} ratio (0.23) equivalent to that of the B-Lode (Table 3), the latter characterized by the assemblage pyrite-magnetite-hematite. The Ti-P isocon almost coincides with the equal-mass diagonal line (Fig. 16d) indicating negligible volume change. Sulfur, K_2O, MnO, CO_2, and Fe_2O_3 are enriched, whereas SiO_2 and Na_2O are slightly and Al_2O_3, CaO, MgO, and H_2O are significantly depleted. The XRD analysis of the mill-head sample indicates that these changes result from the abundance of phengite, quartz, and manganoan ankerite. Albite, siderite, chlorite, and pyrite are minor phases (5–10 vol.%). Hydrothermal magnetite and hematite (≤ 5%) account for the increase in trivalent iron. The selective replacement of albite by phengite + quartz, observed in the outer zone

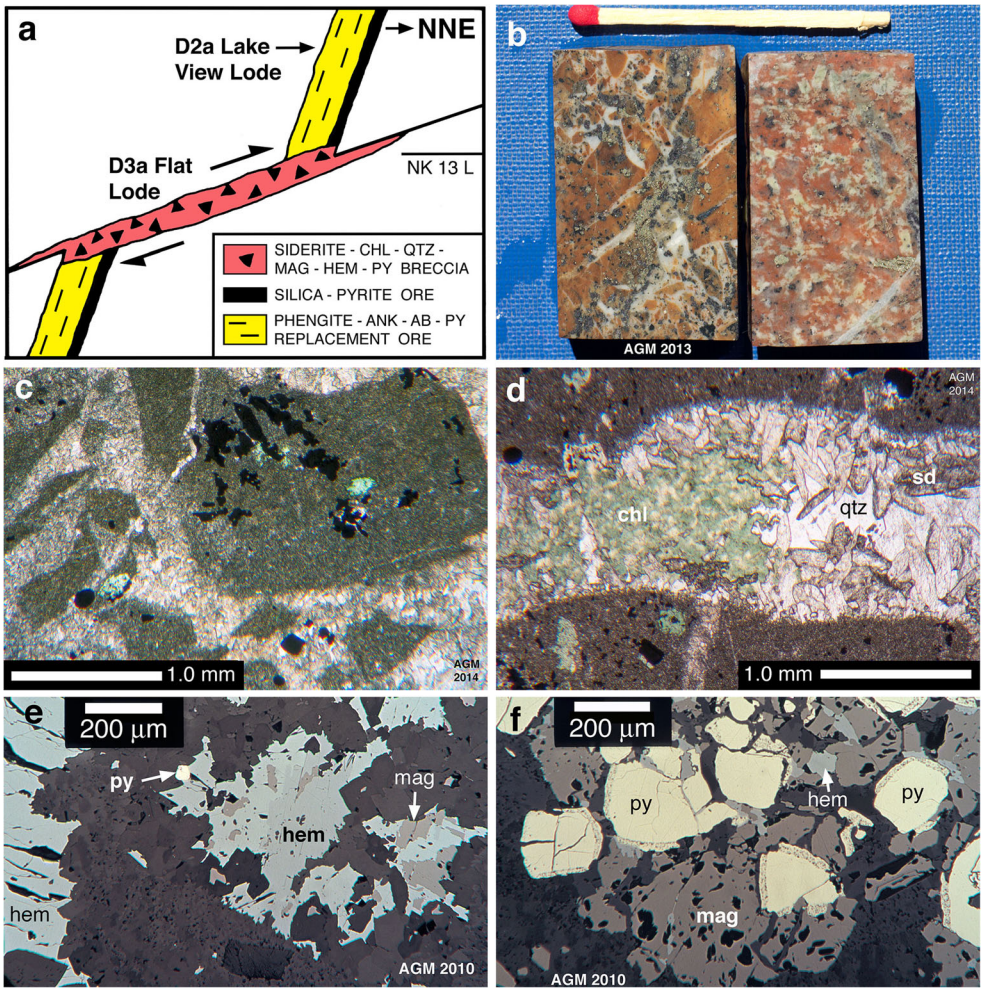

Fig. 15 Structural setting, minerals and textures of Oroya Stage 1 breccia ore from the D3a Flat Lode, North Kalgurli (NK) shaft 13 level (526 m below datum), the host rock is chlorite-calcite altered Golden Mile Dolerite (GMD) Unit 5. **a** Looking northwest at a cross section (not to scale) illustrating the reverse offset of the D2a Lake View Lode at the D3a Flat Lode fault. Minerals: albite (ab), ankerite (ank), chlorite (chl), hematite (hem), magnetite (mag), pyrite (py), quartz (qtz). **b** Breccia ore (left): fragments of hematite-stained massive siderite cemented by white ankerite ± siderite ± quartz ± chlorite. Magnetite, hematite, pyrite, chlorite, and silica replace part of the fragments. Replacement in GMD Unit 5 (right): red mafic sites composed of ankerite ± sericite ± hematite, white plagioclase sites of albite-sericite-quartz, grey igneous quartz, and pink rutile trellis after Ti-magnetite. Disseminated black magnetite and yellow pyrite, veinlet filled with quartz, ankerite and albite. The matchstick is 4 cm long. **c** Fragments of microcrystalline siderite (dark) are partly replaced by magnetite-hematite-pyrite aggregates (opaque), and by chlorite (green) and silica. The ankerite-siderite matrix (light) also contains Fe-oxides and pyrite, plane polarized light. **d** Siderite fragments (dark) cemented by comb-textured ankerite and siderite (sd), and by chlorite (chl) and quartz (qtz), plane polarized light. **e** Specular hematite (hem) in contact with euhedral pyrite (py) replaces magnetite (mag), plane polarized light reflected in air. **f** Pyrite (py) zoned to poikilitic As-rich rims in contact with magnetite (mag). Late hematite (hem) lines the grain boundaries and fractures in pyrite, plane polarized light reflected in air

of the B-Lode (Fig. 4), is the likely cause for the depletion of Na_2O, Al_2O_3, and SiO_2 relative to outer chlorite-calcite altered GMD Unit 9, where albite is stable. The metasomatic changes in lithophile (Fig. 16e) and chalcophile-siderophile trace elements (Fig. 16f) resemble those in the Kelly Lode except that lead is the only base metal enriched. The relative increase of U, Th, and REE is caused by a minor component of GMD Unit 8, which has higher background values than GMD Unit 9 (ESM App. 4).

Oroya-style Blatchford vein

The Blatchford vein above the Paringa South shaft 11 level is hosted by sericite-ankerite altered Paringa Basalt and is zoned from outer chalcedony replacement (30 vol.%) to inner extensional quartz-carbonate fill (70%). The vein sample (1.5 kg) has a low Fe^{3+}/Fe^{2+} ratio (0.03), and its Al/Ti ratio is close to that of the host rock (Table 3). The Al-Ti isocon is shifted to the right of the equal-mass diagonal line (Fig. 16g) due to the large volume gain.

Sulfur and the major oxides are strongly enriched except Na_2O, which is depleted (Fig. 16g). The XRD analysis identified quartz, calcite, and ankerite as principal and muscovite, chlorite, siderite, and pyrite as minor phases (5 vol.% each). Albite was not detected. Relative to the wall rock, all lithophile (Fig. 16h) and all chalcophile-siderophile trace elements (Fig. 16i) are enriched, though some at the sub-ppm

Table 3 Whole-rock major oxide and trace element analyses of D2a Fimiston Lodes (Kelly, B-Lode, LV-PV bulk ore), the telluride vein of the D2b Blatchford Lode (BLF), and the D3a Oroya Hanging Wall (OHW) Lode hosted by Golden Mile Dolerite (GMD) and Paringa Basalt (PB). Lake View (LV), Perseverance (PV) and Paringa South (PS) shafts, Golden Mile, Kalgoorlie

Shaft/level	PS 4L	PS 4L	LV 3L	LV + PV	PS 6L	PS 6L	PS 11L	PS 11L	PS 7L
UWA no.	109705	109706	109737	109738	none	109715	109729	109728	109724
Host rock	GMD 2	GMD 2	GMD 9	GMD 9	GMD 4	PB	PB	PB	PB
Host rock/lode	host	Kelly	host	210,410 t	B-Lode	host	host	BLF	OHW
Alteration/ore	chl-cal	Fimiston	chl-cal	Fimiston	Fimiston	ms-ank	ms-ank	Oroya	Oroya
SiO_2 (wt.%)	44.53	47.36	44.93	44.70	43.31	50.26	43.38	49.18	47.48
TiO_2	0.87	0.56	1.23	1.45	1.07	1.48	1.38	0.23	0.12
Al_2O_3	14.39	9.87	13.20	10.25	15.18	15.69	14.07	3.55	4.72
Fe_2O_3	0.93	0.68	1.37	2.84	2.27	0.21	0.39	0.24	0.52
FeO	10.58	7.72	9.29	11.36	8.55	7.04	9.73	8.18	16.09
MnO	0.15	0.18	0.19	0.23	0.15	0.23	0.28	0.19	0.36
MgO	6.36	4.30	4.31	3.06	3.04	2.17	2.73	1.95	4.25
CaO	7.28	7.89	10.29	6.23	6.17	7.01	8.50	15.32	6.70
Na_2O	1.30	1.78	2.49	2.15	4.27	1.75	0.37	0.00	0.00
K_2O	0.81	1.82	0.25	1.91	2.51	1.55	2.37	0.52	0.31
P_2O_5	0.06	0.04	0.12	0.13	0.07	0.17	0.15	0.07	0.02
L.O.I.	11.79	17.86	11.92	15.30	13.37	12.61	15.49	19.43	19.10
Total	99.04	100.06	99.59	99.58	99.96	100.18	98.84	98.86	99.67
H_2O (wt.%)	5.21	2.72	4.32	1.98	1.65	2.69	2.89	1.31	4.04
CO_2	6.52	10.94	7.54	10.60	7.04	9.70	12.14	15.14	11.56
Sulfur	0.06	4.20	0.06	2.72	4.68	0.22	0.46	2.98	3.50
Fe^{3+}/Fe^{2+}	0.08	0.08	0.13	0.23	0.24	0.03	0.04	0.03	0.03
Density (g/cm^3)	2.81	2.90	2.81	2.93	2.92	n.a.	2.90	2.80	3.01
Ag (ppm)	0.09	5.0	0.04	3.4	11.0	< 0.1	< 0.1	32	3.0
As	13	58	29	174	82	152	144	435	1240
Au	0.024	3.62	0.006	7.00	4.74	0.04	0.46	120	48
Ba	74	150	136	210	170	493	288	138	45
Be	0.4	1.0	n.a.	n.a.	n.a.	0.7	1.2	0.3	0.4
Bi	< 0.1	< 0.1	< 0.01	< 0.01	0.21	0.02	< 0.1	< 0.1	0.1
Co	66	37	47	42	52	49	48	31	24
Cr	129	79	188	39	60	217	249	50	52
Cs	7.6	19	2.8	9	15	7.5	12	4.2	1.6
Cu	43	87	67	74	85	42	30	258	79
Ga	19	12	18	18	n.a.	19	21	8	12
Hf	1.3	1.1	1.9	2.7	2.0	2.7	2.4	0.9	1.5
Hg	0.03	4.26	0.04	3.13	2.85	0.04	0.08	40	11
Li	213	6.5	110	21	4.4	55	59	9.8	24
Mo	0.1	1.5	0.1	5.0	0.2	0.6	0.4	0.5	1.1
Nb	2.9	2.1	3.16	3.7	1.8	6	5.4	1.4	3.4
Ni	239	110	67	37	35	86	93	56	44
Pb	0.5	3.8	5	16	10	10	6	49	31
Rb	37	76	15	61	58	49	85	26	16
Sb	4.9	8.8	1.3	23	6.6	2.4	3.8	66	7.7
Sc	28	24	51	37	n.a.	30	32	24	36
Se	0.2	2.4	0.3	1.4	2.3	< 2	0.3	1.8	2.4
Sn	< 0.5	2.1	0.5	1.6	0.6	0.9	< 0.5	< 1	< 1
Sr	73	107	94	167	145	369	150	294	69
Ta	0.6	0.5	1.1	1.2	0.43	0.51	0.9	< 0.1	0.7
Te	< 0.1	15	0.3	9.4	17	< 0.1	1.4	138	69

Table 3 (continued)

Shaft/level	PS 4L	PS 4L	LV 3L	LV + PV	PS 6L	PS 6L	PS 11L	PS 11L	PS 7L
UWA no.	109705	109706	109737	109738	none	109715	109729	109728	109724
Host rock	GMD 2	GMD 2	GMD 9	GMD 9	GMD 4	PB	PB	PB	PB
Host rock/lode	host	Kelly	host	210,410 t	B-Lode	host	host	BLF	OHW
Alteration/ore	chl-cal	Fimiston	chl-cal	Fimiston	Fimiston	ms-ank	ms-ank	Oroya	Oroya
Th	0.3	0.1	0.44	0.81	0.44	1.4	1.4	2.3	5.1
Tl	0.02	0.08	< 0.01	0.15	0.10	0.57	0.10	0.13	0.12
U	< 0.1	0.25	0.11	0.24	0.14	0.5	0.4	0.5	1.3
V	268	267	451	465	320	329	310	437	294
W	3.2	16	1.0	60	15	n.a.	8.1	3.8	12
Y	19	16	25	34	n.a.	22	25	15	33
Zn	126	23	80	115	101	66	117	245	511
Zr (ICP-MS)	51	35	60	86	69	97	95	30	50
Zr (XRF)	60	45	75	103	75	94	104	47	59
Total REE	33.29	25.36	35.13	61.82	37.54	39.74	58.7	47.1	81.18
Al/Ti ratio	5.25	5.59	3.40	2.25	4.50	3.36	3.23	4.90	12.48
Ti/P ratio	3.79	3.66	2.68	2.91	4.00	2.28	2.41	0.86	1.57
Ti/Zr ratio	86.93	74.60	98.32	84.10	85.53	94.39	79.55	29.34	12.19
Zr/Hf ratio	39.23	31.82	31.58	31.96	34.50	35.93	39.58	33.33	33.33

Minerals: ankerite (ank), calcite (cal), chlorite (chl), muscovite (ms). The analytical methods are listed in Appendix 2 of the Electronic Supplementary Material. Detection limits: major oxides, carbon dioxide and sulfur 0.01–0.05 wt.%. As, Co, Cr, Cu, Ga, Ni, Pb, Rb, Sc, Sr, V, Y, Zn, Zr by XRF 1–5 ppm. Au by fire assay 0.005 ppm, Hg by cold vapor AAS 0.01 ppm. REE, Nb, Ta, Th, U by ICP-MS fusion 0.05–0.1 ppm, other trace elements by ICP-MS acid digest 0.01–0.1 ppm. Below detection (ppm): Pt (< 0.1), Re (< 0.01)

n.a. not analyzed, *UWA no.* sample number of the Clarke Earth Science Museum, the University of Western Australia (Mueller 1990)

level (Be, U, Mo, Tl). The enrichment is related to substitution in muscovite and chlorite (Li, Cr, Ga, V), carbonate (Sr), rutile (W, Nb, V), and in apatite, monazite, and xenotime (P_2O_5, REE, Y, Th, U). Total P_2O_5 in the vein is low (0.07 wt.%). Ore minerals causing enrichment include: native gold and tellurides (Au, Ag, Hg, Pb, Te, Se), chalcopyrite (Cu), sphalerite (Zn), arsenopyrite (As, Sb), and pyrite (Ni, Co).

Oroya Hanging Wall Lode

The Oroya Hanging Wall (OHW) Lode, sampled in bulk (2 kg) on the Paringa South shaft 7 level (Fig. 13), is located in a dilated flat section of the reverse shear zone (Mueller 2017, this issue). The Fe^{3+}/Fe^{2+} ratio of the ore is low (0.03), and its Ti/P ratio is close to that of sericite-ankerite altered Paringa Basalt (Table 3). A large volume gain is indicated by the shift of the Ti-P isocon (Fig. 16j).

Sulfur and the major oxides are enriched except for Na_2O, which is depleted (Fig. 16j). Most remarkable are the strong enrichment in FeO (ankerite, siderite, pyrite), SiO_2 (chert-like quartz), and sulfur (pyrite) and the distinct enrichment in Al_2O_3 (chlorite) and K_2O (muscovite). The XRD analysis confirms that quartz, ankerite, and chlorite are main constituents, pyrite and siderite are major (about 10 vol.%), and muscovite is minor (5%). Albite is absent.

Most lithophile (Fig. 16k) and chalcophile-siderophile trace elements (Fig. 16l) are enriched, and only Ba, Cs, and Tl show no change or slight depletion. Once again, the elements enriched may be grouped according to substitution in: muscovite and chlorite (Li, Rb, Ga, Cr, V), ankerite (Sr), rutile (Nb, Ta, Sc?), apatite, monazite and xenotime (REE, Y, Th, U), native gold and tellurides (Au, Ag, Hg, Pb, Te, Se), chalcopyrite (Cu), sphalerite (Zn), arsenopyrite (As, Sb), pyrite (Ni, Co), and scheelite (W, Mo). The P_2O_5 content of the ore is low (0.02 wt.%; Table 3).

Residual minerals

Titanium residing in rutile is part of all isocons in combination with phosphorus and aluminium. Relative to these isocons, zirconium and hafnium are immobile in Fimiston replacement ore. In contrast, both are enriched in the OHW Lode and in the Blatchford vein (Fig. 16). The Zr/Hf ratios of wall rock and ore, however, vary within narrow limits (Table 3) suggesting that zircon inherited from the wall rock rather than hydrothermal zircon is the main Zr-Hf mineral.

In the OHW Lode, Al_2O_3 is also enriched consistent with the abundance of chlorite. Relative to Ti, the enrichment factors calculated are Al (2.7×), Ga (6.8×), Zr (6.7×), and Hf (5.9×). If these elements are residual, concentrated in

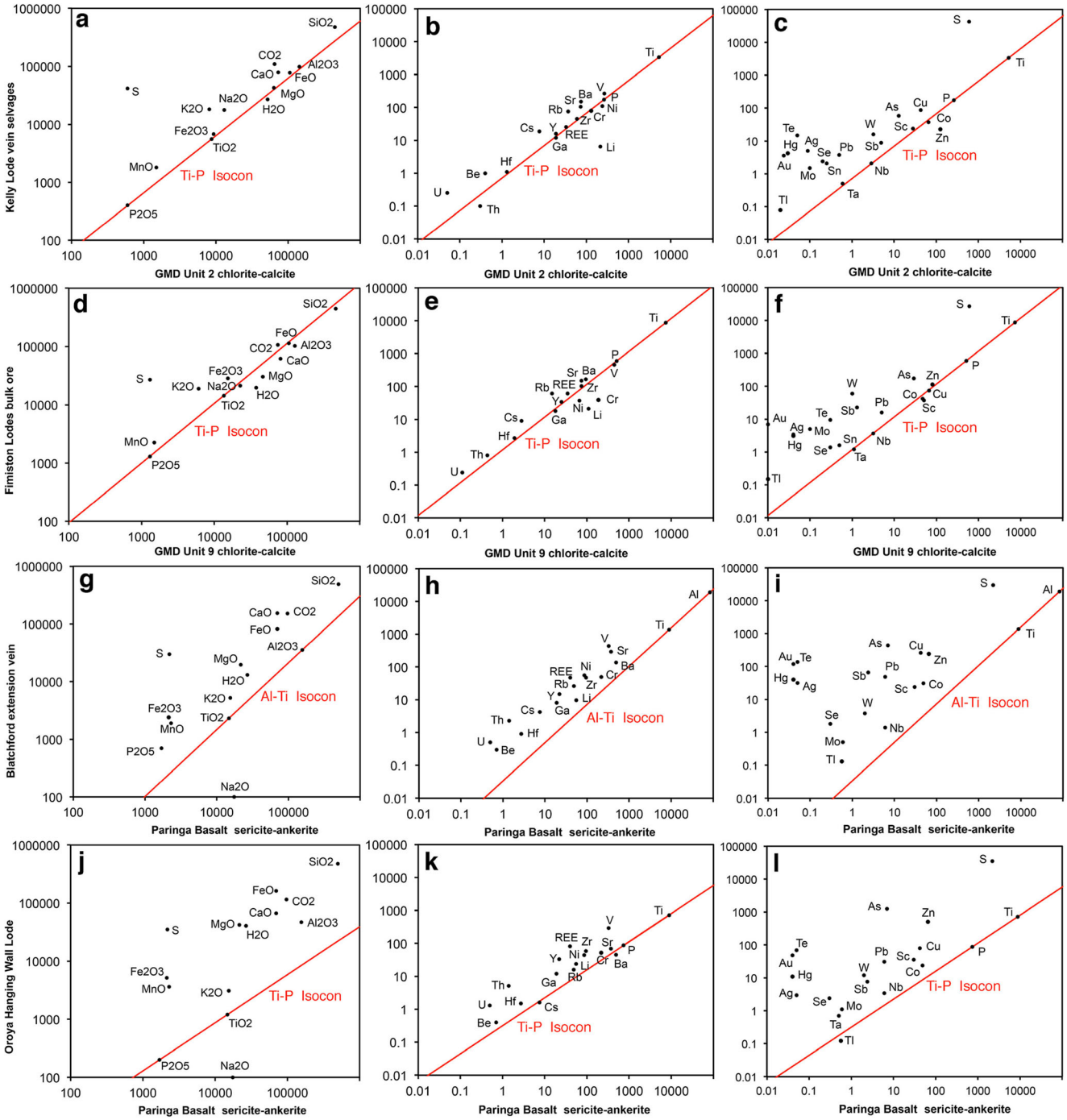

Fig. 16 Isocon diagrams after Grant (1986) illustrating the metasomatic changes in Fimiston- and Oroya-style gold ore relative to outer chlorite-calcite altered Golden Mile Dolerite (GMD) or sericite-ankerite altered Paringa Basalt (PB), Golden Mile, Kalgoorlie. The analytical data are listed in Table 3. **a** D2a Kelly Lode, Fimiston-style, Paringa South shaft 4 level: major oxides in pyrite-rich vein selvages relative to GMD Unit 2 below the lode, sample numbers UWA 109705 and 109706. **b** Kelly Lode: lithophile trace elements. **c** Kelly Lode: chalco- and siderophile trace elements. **d** D2a Fimiston Lodes, Lake View and Perseverance shafts: major oxides of mill-head sulfide ore (240,410 t; UWA 109738) relative to the average propylitic GMD Unit 9 (ESM App. 2b). **e** Fimiston Lodes: lithophile trace elements, UWA 109737 and 109738. **f** Fimiston Lodes: chalco- and siderophile trace elements, UWA 109737 and 109738. **g** D2b Blatchford extension vein, Paringa South shaft 11 level: major oxides of Oroya-style vein material (1.5 kg; UWA 109728) composed of Stage 1 chalcedony replacement (30 vol.%) and Stage 2 quartz-carbonate fill (70%) relative to altered PB (UWA 109715). **h** Blatchford vein: lithophile trace elements. **i** Blatchford vein: chalco- and siderophile trace elements. **j** D3a Oroya Hanging Wall (OHW) Lode, Paringa South shaft 7 level: major oxides of Oroya-style Stage 1 and Stage 2 ore (2 kg; UWA 109724) relative to altered PB (UWA 109715). **k** OHW Lode: lithophile trace elements. **l** OHW Lode: chalco- and siderophile trace elements

chlorite-muscovite ± rutile ± zircon stylolites, then lode formation will include processes such as extensional fill, silica replacement and wall-rock dissolution, the latter indicated by the nodular "cavity-fill" veins in the central part of the lode (Fig. 13).

Discussion

Wall-rock alteration in the Golden Mile has been linked to regional metamorphism during fold-belt evolution (e.g., Witt 1991; Goldfarb et al. 2005), and classified as "mesozonal" (6–12 km crustal depth; Groves 1993) emphasizing the P-T conditions of the metamorphic terrane. As such classification is less useful at the scale of the ore bodies, the base-cation leaching concept of Meyer and Hemley (1967) is introduced. The km-scale paragonite-chloritoid zone at the southeast margin of the Golden Mile is discussed first and compared to similar zones associated with other gold deposits in the Eastern Goldfields Province. The sequence of wall-rock alteration and mineralization in the Golden Mile is summarized in Fig. 17. The results of the Paringa South case study are discussed in the context of published data from other parts of the deposit.

Classification of wall-rock alteration

Wall-rock alteration is subdivided according to the degree of feldspar destruction by base-cation leaching (hydrolytic alteration), an approach emphasizing fluid-wall rock interaction without assumptions about the fluid source (Meyer and Hemley 1967; Rose and Burt 1979). In this context, the chlorite-calcite ± epidote zone enveloping the Golden Mile deposit represents hydrous "propylitic" alteration because albite is stable and abundant. As ankerite is the main carbonate in all ore bodies, white mica remains as the most distinctive gangue mineral in Fimiston Lodes and the Trafalgar Fault zone. In both, hydrolytic alteration predominates involving muscovite-phengite/paragonite-quartz replacement of albite, apart from albite-stable central structures. Albite is absent in ore replacing sericite-ankerite altered Paringa Basalt suggesting that albite-rich propylitic GMD is required as a buffer to stabilize feldspar. Oroya-style ore is characterized by the deposition of silica and chlorite coupled with iron enrichment, and represents combined silicification and "chloritic alteration" in the sense of Meyer and Hemley (1967).

Trafalgar Fault paragonite-ankerite-chloritoid zone

In the Golden Mile, km-scale propylitic alteration (310–340 °C; Fig. 17) overprints the metamorphic actinolite-albite-zoisite assemblage in the tholeiitic host rocks (Travis et al. 1971; Phillips 1986). Zones of sericite-ankerite and chlorite-ankerite alteration, tens of meters wide and variably mineralized with magnetite ± hematite, replace the chlorite-calcite assemblage in parts of the Golden Mile Dolerite and in Paringa Basalt at the GMD contact. Though anomalous in gold (20–200 ppb), these early ankerite zones are crosscut by the ore bodies and predate main-stage sulfide deposition (Clout et al. 1990). They are broadly synchronous with the emplacement of diorite porphyry dykes at 2663 ± 11 Ma (Fig. 17).

In the Trafalgar Fault at the southeast margin of the Golden Mile, the abundance of paragonite and chloritoid contrasts with the predominance of phengite, muscovite or chlorite in all lodes of the deposit. Yet, the zonation from albite-stable alteration in the D2a Trafalgar Fault to paragonite-quartz in the outer hydrolytic zone resembles the lateral zonation in the Paringa B-Lode. Other similarities to D2a Fimiston Lodes include the lack of iron enrichment, the metasomatic addition of K_2O, CO_2, S, Ba, Sr, Rb, Cs, As, and Sb (ESM App. 3), and the assemblage pyrite-chalcopyrite ± magnetite ± hematite. For these reasons, the alteration zone of the Trafalgar Fault is correlated with Fimiston ore formation (Fig. 17). Striking differences are the low gold grade (48–75 ppb; ESM App. 2b), and the lack of iron oxides in the fault. Anhydrite or gypsum were not detected but may be leached below the saprolite (Fig. 2b).

The barren sericite-ankerite zone bound to the GMD-PB contact in the Kalgoorlie Anticline plunges 20° SE and merges with the paragonite-ankerite-chloritoid zone of the Trafalgar Fault (Fig. 2a). A lateral zonation in mineral composition within the contact zone is not documented. Muscovite and paragonite are both present at the Paringa South shaft where chloritoid is absent. Temperature estimates averaging 410 °C suggest that the Trafalgar Fault alteration zone constitutes a thermal anomaly within the wider propylitic envelope (310–340 °C; Fig. 17).

In the Charlotte vein stockwork at Kalgoorlie, the auriferous vein selvage changes from muscovite-ankerite-pyrite at surface to albite-ankerite-pyrrhotite 1 km below. Gold grade decreases inversely with temperature (Mueller 2015). This vertical transition from high-temperature Na-rich to distal K-rich alteration may be analogous to the lateral one in the Golden Mile.

Paragonite-chloritoid alteration in the Eastern Goldfields

Elsewhere in the Eastern Goldfields Province, chloritoid and paragonite are common in zones centered on inner quartz-sericite-pyrophyllite ± andalusite-kyanite alteration (Fig. 1). In the Leonora area north of Kalgoorlie, km-scale hydrothermal alteration overprints 2.8 Ga greenschist facies komatiite and basalt east of the 2.75 Ga Raeside granite batholith (see

the map in ESM App. 6). Gold deposits are located at the contacts of the batholith and its satellite plutons (Duuring et al. 2004). The zircon U-Pb ages of altered diorite-granodiorite dykes at Tarmoola (2667 ± 8 Ma; Fletcher et al. 2001) and at Tower Hill (2670 ± 5 Ma; Dunphy et al. 2003) set maximum time limits for mineralization.

The Sons of Gwalia deposit (179 t Au to 2017) replaces actinolite-albite meta-basalt overprinted by propylitic chlorite-calcite alteration. The pipe-shaped ore body plunges 40–45° E, and consists of biotite-calcite-pyrrhotite and quartz-rich sericite-dolomite-pyrite schist (8.4 g/t Au). North of this deposit, broad zones of chloritoid-chlorite-sericite-quartz and inner quartz-paragonite-andalusite ± kyanite schist are exposed at Mount Leonora (ESM App. 6). The Al-silicates are intergown with natro-alunite and are rimmed by pyrophyllite, which is in contact with kaolinite in the sulfide zone (Hallberg 1983). Ankerite and pyrite, and accessory chalcopyrite, tennantite, pyrrhotite, gersdorffite, and arsenopyrite are

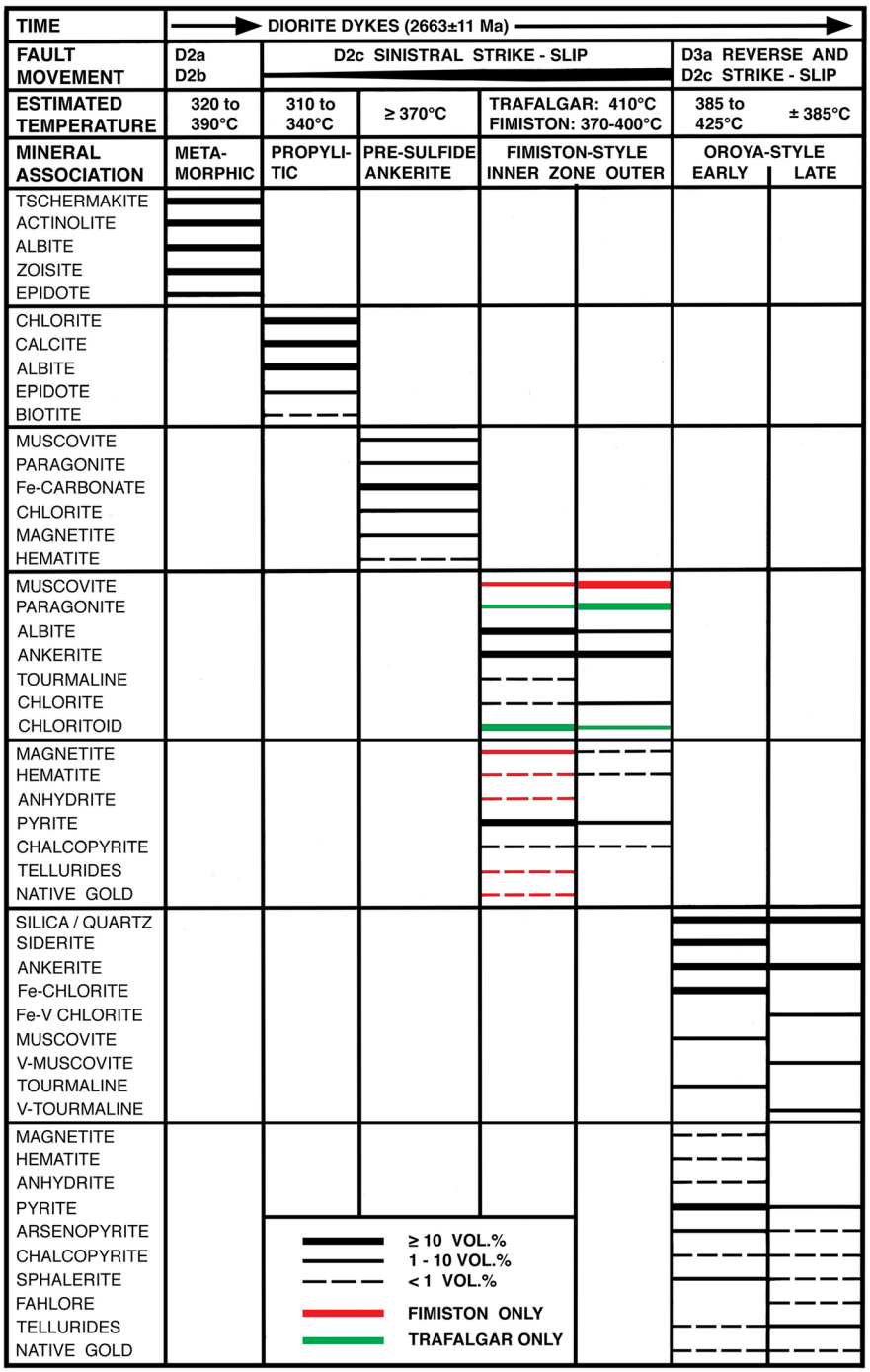

Fig. 17 Time-line diagram summarizing the sequence of wall-rock alteration and gold mineralization in the Golden Mile deposit, Kalgoorlie. Fault movement and diorite porphyry emplacement are according to Mueller (2017, this issue). The metamorphic mineral assemblages and temperatures are from Goscombe and Blewett (2009) and the propylitic assemblages from Stillwell (1929), Bartram and McCall (1971), and Clout et al. (1990). Oroya-style mineralization is absent in the D2a Trafalgar Fault, overprints Fimiston ore in many D2a and some D2b faults, and is the only ore type in D3a reverse faults. Data on alteration minerals and estimated temperatures are listed in Table 1 and ESM App. 1. The term "silica" denotes chert-like quartz and chalcedony, and the term "fahlore" the tetrahedrite-tennantite series

disseminated (Skwarnecki 1990). P-T conditions of > 250 MPa and 380–470 °C are indicated by late kyanite in contact with andalusite, and by the absence of sillimanite and the assemblages staurolite-quartz, almandine-staurolite, and almandine-albite. Retrograde pyrophyllite and kaolinite-quartz suggest that the temperature declined first to 350 °C and then to 250 °C (see P-T diagram in ESM App. 7). Hallberg (1983) interprets the Mount Leonora zone as hydrothermal, a conclusion consistent with zircon U-Pb chronology.

The occurrence of natro-alunite is intriguing, as this mineral is characteristic of "advanced argillic alteration" in the sense of Meyer and Hemley (1967). The andalusite- and kyanite-bearing zone at Mount Leonora may represent the high-PT equivalent of this alteration type. The sulfide assemblage, however, indicates a sulfidation state well below that of high-level Au-Ag-Cu deposits (e.g., Einaudi et al. 2003). At the southeast margin of the Golden Mile, there is no evidence of a high-PT advanced argillic zone. If present, it must be located at depth and northeast of the Trafalgar Fault.

Previous studies of Golden Mile ore

Mineralization styles in the Golden Mile outside the Paringa South mine are summarized in Clout et al. (1990) as follows: (1) outer ankerite-dolomite replacement; (2) inner grey pyrite-rich sericite-ankerite ore, locally associated with (2a) Green Leader marked by V-muscovite and tellurides; and (3) inner siliceous ore (> 80% quartz). Most ore bodies are brecciated and variably mineralized with pyrite, magnetite, hematite, and anhydrite. The "lode alteration" of Gauthier (2006) comprises three successive stages: (1) Fimiston-style ankerite-sericite replacement, 10–20 vol.% pyrite + magnetite, gold, and tellurides as inclusions in pyrite; (2) Green Leader comb-textured and brecciated quartz-ankerite veins with silica-pyrite replacement selvages, vanadian muscovite, free tellurides and gold, and local anhydrite ± hematite; and (3) quartz-ankerite veins with sericite-ankerite-pyrite selvages.

These mineralization schemes are compatible with the results of this study suggesting that the ore bodies described are representative of the broader Golden Mile. Fimiston-style refractory pyrite ore constitutes the Paringa B-Lode and the Kelly Lode, both overprinting propylitic Golden Mile Dolerite, and forms part of the Blatchford Lode replacing sericite-ankerite altered Paringa Basalt. Non-refractory Oroya-style ore is represented by the North Kalgurli Flat Lode and by the Oroya Hanging Wall (OHW) and Blatchford lodes in the Paringa South mine. The latter two are composed of the early pyrite and late telluride stages described from silicified lodes in other parts of the Golden Mile (Tomich 1952).

Fluid inclusion studies summarized in Ho et al. (1990) show that the aqueous fluid trapped in Fimiston- and Oroya-style vein quartz is CO_2-rich ($X_{CO2} = 0.15$), of low to moderate salinity (2–5.5 wt.% $NaCl_{eq}$), and of high density (0.75–0.95 g/cm^3). Methane was detected in veins where the OHW Lode intersects altered carbonaceous greywacke (local fluid: 70–85 wt.% H_2O, 10–25% CO_2, 1–5% CH_4). Median homogenization temperatures not corrected for pressure vary from 220 to 315 °C and median isochore pressures from 200 to 300 MPa. At lithostatic load, a pressure of 300 MPa converts to a depth of about 10 km (3.6 km per 100 MPa at 2.85 g/cm^3 density; Bucher and Frey 2002), a deep crustal level of ore formation.

Fimiston ore in the Paringa South mine

Fimiston refractory ore (4–20 g/t Au) occurs in D2a (B-lode, Kelly Lode) and in D2b shear zones (Blatchford Lode) reactivated during D2c sinistral strike-slip. In lodes hosted by propylitic GMD, albite is stable in brittle fault-fill veins and in the innermost vein selvage. Tourmaline and fluor-apatite are accessories. Phengitic muscovite (< 0.2 wt.% V_2O_3) is common in the selvage but increases in the outer hydrolitic zone where phengite + quartz selectively replace albite (B-Lode). Chlorite temperature estimates are 390–400 °C for the vein selvage and 370 °C for the outer hydrolytic zone. Ankerite is the dominant carbonate. In lodes located within the pre-sulfide Paringa Basalt contact zone, S-C mylonite composed of muscovite-ankerite-quartz ± tourmaline traces the shear zones.

The pyrite is either zoned in arsenic content (B-Lode, Blatchford) or is arsenic poor (Kelly Lode). Accessory chalcopyrite is ubiquitous, sphalerite is absent, and tennantite is associated with arsenical pyrite. Sulfide and sulfide-oxide assemblages define an intermediate sulfidation state. Fimiston ore requires roasting because native gold and tellurides occur as inclusions (mostly 1–5 μm) in pyrite. Hessite, petzite, coloradoite, and melonite were detected in B-Lode and Kelly Lode pyrite. The Au/Ag ratios of ore from the B-Lode (0.43), Kelly Lode (0.72), and the Fimiston mill-head (2.06) suggest that gold inclusions predominate but that Au-Ag tellurides are abundant locally.

The strong enrichment of sulfur in the bulk mill-head sample (210,410 t) illustrates the abundance of pyrite in both the inner albite-stable and outer hydrolytic zone of Fimiston Lodes. According to the mass-balance calculations, the ore fluid introduced significant amounts of Mn, Ca, K, CO_2, and sulfur but did not add iron and magnesium. Large-ion lithophile elements (Ba, Rb, Cs), strontium, and the chalcophile-siderophile elements Au, Ag, Hg, Te, Se, Cu, Pb, As, Sb, Mo, and W were also introduced. Lithium may form an outer geochemical halo (110–213 ppm; Table 3) in propylitic GMD adjacent to lodes.

Oroya ore in the Paringa South mine

Oroya-style pyrite-telluride mineralization overprints Fimiston ore in the D2b Blatchford Lode, and is the only ore

in the D3a reverse faults controlling the North Kalgurli Flat Lode and the Paringa OHW Lode. The structural relations indicate a hiatus between the Fimiston and Oroya hydrothermal systems. Oroya mineralization is subdivided into Stage 1 silica-chlorite-siderite-pyrite and Stage 2 silica-ankerite-pyrite-telluride ore. In the Flat Lode (5 g/t Au), Stage 1 ore was deposited at 385 °C and Stage 2 is absent. In the OHW and Blatchford Lodes, fluid temperature is estimated at 400–425 °C during Stage 1 and at 385 °C during Stage 2. Early silica and chalcedony are colored dark by dispersed micron-sized pyrite. Fe-chlorite, muscovite and tourmaline are low in vanadium (≤ 0.25 wt.% V_2O_3). During Stage 2, pure silica, comb-textured quartz in veins and breccia, green vanadian muscovite, red Fe-V chlorite, red tourmaline (all > 0.5 wt.% V_2O_3), and fluor-apatite were deposited. The presence of chalcedony has been interpreted to indicate a shallow crustal level of ore formation (Gauthier et al. 2007), in disagreement with the fluid inclusion pressure estimates (Ho et al. 1990). Rapid cooling during each stage and/or precipitation from fluid super-saturated in silica may be alternative interpretations.

In contrast to Fimiston, Oroya ore is not refractory. In the OHW and Blatchford lodes, free gold is associated with pyrite, arsenopyrite, sphalerite, chalcopyrite, tetrahedrite and melonite, and a late Sb- and Pb-rich telluride assemblage comprising montbrayite, tellurantimony, coloradoite, altaite, calaverite, and petzite. The sulfidation state increased with time from low (pyrite-pyrrhotite-arsenopyrite) to intermediate (pyrite-chalcopyrite-tetrahedrite) to high (covellite-digenite), perhaps coincident with decreasing temperature. The local presence of calaverite and native tellurium (Scantlebury 1983) indicates a high tellurium fugacity, at least at the onset of telluride deposition (see Afifi et al. 1988).

The OHW Lode and Blatchford vein are extensional structures hosted in altered Paringa Basalt. Mass-balance calculations indicate that the ore fluid added significant amounts of silica, Fe, Mg, Mn, Ca, K, CO_2, and sulfur, lithophile Li, Rb, Sr, and Ga, siderophile Cr, Ni, V, and W, and chalcophile Au, Ag, Hg, Te, Cu, Zn, Pb, As, Sb, Co, and Se. Sodium is the only major element depleted in the ore.

Oxidized versus reduced ore bodies

Fimiston ore in the B-Lode is characterized by the oxidized assemblage pyrite-magnetite-hematite ($Fe^{3+}/Fe^{2+} = 0.24$), whereas the lateral termination of the Kelly Lode lacks iron oxides ($Fe^{3+}/Fe^{2+} = 0.08$). A surprising result is the oxidized nature of the bulk Fimiston ore (240,410 t) indicated by the high Fe^{3+}/Fe^{2+} ratio (0.23) and enrichment of Fe_2O_3 in the mill-head sample (Fig. 16d). This suggests the widespread occurrence of magnetite and hematite in Fimiston Lodes controlled by the main D2a shear-zone system. The high oxidation state inferred is supported by negative $\delta^{34}S$ median values in pyrite (− 5.1 to − 5.5‰; $n = 46$) and positive values (+ 12.0 to + 19.2‰; $n = 7$) in co-genetic anhydrite (Clout et al. 1990; Golding et al. 1990). Oroya-style ore also varies in oxidation state from high in the Flat Lode (hematite stable) to low in the OHW and Blatchford lodes ($Fe^{3+}/Fe^{2+} = 0.03$; no Fe-oxides). The reduced nature of the pyrrhotite-bearing ore bodies may be related to organic methane released from local black schist. Flat Lode pyrite also has a negative $\delta^{34}S$ signature of − 4.7‰ ($n = 22$; Golding et al. 1990).

The sulfide-sulfate relations have been interpreted to reflect the infiltration of a reduced fluid oxidized by reaction with Ti-magnetite in the Golden Mile Dolerite, which deposited hematite after cooling from about 450 °C to less than 280 °C (Evans et al. 2006). This process requires a low fluid/rock ratio (0.1 to 5), a higher Fe^{3+}/Fe^{2+} ratio (0.20) than measured in propylitic GMD Unit 9 (0.13; Bartram and McCall 1971), and inward flow from outer alteration zones into the lode structures to deposit the tens of million tons of pyrite mined (Evans et al. 2006). These constraints are inconsistent with the results of this study because (1) zoned lode alteration progressively replaces previously altered wall rock (outward flow), (2) the lode terminations (Kelly Lode) are more reduced rather than oxidized (lateral flow), and (3) the temperature of the ore fluid was higher than permitted for hematite deposition in the rock-buffered system modeled.

Constraints on fluid sources

The Golden Mile ore bodies result from the superposition of two hydrothermal systems separated in time by D3a reverse faulting. The younger Oroya system deposited abundant tellurides after most of the pyrite, a sequence common in magmatic hydrothermal ore deposits (Afifi et al. 1988). The vast volume of hydrous altered rock suggests a fluid-buffered system requiring significant dissolved SO_2-SO_4 relative to H_2S to account for the oxidized nature of many Golden Mile lodes. These constraints favor a felsic magmatic source, as Archean surface water and metamorphic fluid ascending through thick ferrous greenstones were both reduced (e.g. Cameron and Hattori 1987). Along the Boulder Lefroy fault system controlling the Golden Mile deposit, anhydrite-bearing gold deposits at Kambalda (Bath et al. 2013), Cu-Au epidote-magnetite endoskarns at Hannan South and Mt Shea (Mueller et al. 2012), and monzodiorite-granodiorite intrusive complexes all formed during the period 2663 ± 11 to 2651 ± 9 Ma (Mueller 2007, 2017). Gravity lows and reflection seismic sections outline plutons as the source of dykes and oxidized hydrothermal fluid beneath mineralized faults (Neumayr et al. 2008; Bath et al. 2013; Mueller et al. 2016, this issue). Strontium is enriched in both Fimiston- and Oroya-style ore. The initial $^{87}Sr/^{86}Sr$ ratios of monzodiorite-suite porphyries and associated lamprophyres (0.7014–0.7018) match those recorded in tourmaline from the Kelly Lode (0.7014), in scheelite from the OHW Lode (0.7018; Mueller et al. 1991),

and in anhydrite from Fimiston Lodes (0.7013–0.7016; Cameron and Hattori 1987). The initial ratios of the mantle-derived tholeiitic host rocks are lower (0.7009–0.7011; Faure 2001).

Conclusions

(1) Prior to gold mineralization, hydrothermal fluid infiltrating the vast Golden Mile shear-zone system generated hydrous propylitic alteration at 310–340 °C in tholeiitic Golden Mile Dolerite (GMD) and Paringa Basalt (PB), and barren ankerite-sericite-chlorite ± magnetite zones in fractured GMD and at the GMD-PB contact of the Kalgoorlie Anticline.

(2) The ankerite-muscovite ± paragonite ± chlorite zone at the GMD-PB contact extends from the Paringa South mine 1.5 km southeast, where it merges with the km-scale paragonite-ankerite-chloritoid zone in GMD centered on the Trafalgar Fault. Chloritoid-bearing alteration is zoned from albite stable in the fault to outer hydrolytic paragonite-quartz replacement. Pyrite ± chalcopyrite mineralization is of low grade (< 0.1 g/t Au). Temperature estimates of 405–425 °C indicate that the paragonite-ankerite-chloritoid zone represents a thermal anomaly in propylitic GMD (< 350 °C) at the periphery of the deposit.

(3) Fimiston-style refractory pyrite ore formed by replacement of altered GMD and PB in D2a and D2b shear zones. In propylitic GMD, narrow albite-stable zones centered on veins give way to outer hydrolytic phengite-quartz alteration. Ore bodies are characterized by the oxidized assemblages pyrite-magnetite and pyrite-hematite ± anhydrite but lack iron oxides at their lateral termination. Most pyrite is arsenical and associated with minor chalcopyrite and tennantite. Sphalerite is absent. Native gold and Au-Ag tellurides form micron-sized inclusions in pyrite. The ore fluid introduced mainly Ca, K, CO_2, S, Ba, Rb, Cs, and Sr but not Fe. Pyrite and gold precipitated at 370–400 °C during the sulfidation of iron in the wall rock.

(4) Oroya-style pyrite-telluride ore formed by silicification and by chlorite-siderite-ankerite ± tourmaline replacement. It overprints Fimiston ore in D2a and D2b shear zones and is the only ore in D3a reverse faults. Ore bodies vary from oxidized (5 g/t Au; pyrite-hematite) to reduced (50–120 g/t Au; pyrite-pyrrhotite). Trapped methane derived from local black schist acted as a reducing agent. In the Paringa South mine, early arsenic- is distinguished from late antimony-rich mineralization. Stage 1 ore (400–425 °C) composed of pyrite (15 vol.%), minor arsenopyrite, sphalerite, chalcopyrite, and free gold is crosscut by Stage 2 (385 °C) comprising pyrite (5%), minor tetrahedrite, montbrayite, tellurantimony, coloradoite, altaite, and gold associated with V-muscovite, Fe-V chlorite, and V-tourmaline. The ore fluid introduced mainly silica and iron, and lesser Mg, Mn, Ca, K, CO_2, S, Te, Li, Rb, Sr, Ga, Cr, Ni, and V.

(5) The Fimiston and Oroya hydrothermal systems are separated in time. The Fimiston fluid infiltrated only D2a and D2b shear zones during D2c strike-slip reactivation. The Oroya fluid infiltrated the D2a and D2b shear-zone system, and D3a reverse faults offsetting the latter. Both fluids were oxidized and became reduced during interaction with the iron-rich wall rocks and/or trapped organic methane. Both were CO_2-rich and of low to moderate salinity, consistent with a confining pressure of about 300 MPa, and both introduced Ca, K, Rb, Sr, and sulfur. The fluid of the younger Oroya system differed by larger amounts of dissolved silica, Fe, Cr, Ni and V, and by its evolution to a high tellurium fugacity evident in the deposition of calaverite and native tellurium.

Acknowledgments The author acknowledges the receipt of a scholarship during his Ph.D. study at the University of Western Australia. Ray Chang assisted with the XRD and XRF analyses and Malcolm Roberts during the electron microprobe sessions at the Centre for Microscopy, Characterization and Analysis (CMCA), the University of Western Australia. Scott Halley kindly measured the SWIR absorption spectra of representative samples. Greg Hall and Patrick Verbeek, former Gold Resources Pty Ltd of the CSR Paringa Project, encouraged mapping in the Paringa South underground mine before closure in 1987. The manuscript benefitted from improvements suggested by Stephen Kesler and David Craw.

References

Afifi AM, Kelly WC, Essene EJ (1988) Phase relations among tellurides, sulfides and oxides: II. Application to telluride-bearing ore deposits. Econ Geol 83:395–404

Bartram GD, McCall GJH (1971) Wall-rock alteration associated with auriferous lodes in the Golden Mile, Kalgoorlie. In: Glover JE (ed) Symposium on Archaean rocks. Geol Soc Australia, Spec Pub 3, pp 191–199

Bath LB, Walshe JL, Cloutier J, Verrall M, Cleverley JS, Pownceby MI, Macrae CM, Wilson NC, Tunjic J, Nortje GS, Robinson P (2013) Biotite and apatite as tools for tracking pathways of oxidized fluids in the Archean East Repulse gold deposit, Australia. Econ Geol 108: 667–690

Bucher K, Frey M (2002) Petrogenesis of metamorphic rocks, 7th edn. Springer, Berlin, 341 pp

Cameron EM, Hattori K (1987) Archean gold mineralization and oxidized hydrothermal fluids. Econ Geol 82:1177–1191

Cassidy KF, Champion DC, Krapez B, Barley ME, Brown SJA, Blewett RS, Groenewald PB, Tyler IM (2006) A revised geological framework for the Yilgarn Craton, Western Australia. Geological Survey of Western Australia, Record 2006/8, 8 pp

Cathelineau M (1988) Cation site occupancy in chlorites and illites as a function of temperature. Clay Minerals 23:471–485

Chang LLY, Howie RA, Zussman J (1998) Non-silicates: sulphates, carbonates, phosphates, halides. Rock-forming minerals Volume 5B, 2nd ed. The Geological Society, London

Clout JMF, Cleghorn JH, Eaton PC (1990) Geology of the Kalgoorlie goldfield. In: Hughes FE (ed) Geology of the mineral deposits of Australia and Papua New Guinea. Melbourne, Australasian Institute of Mining and Metallurgy, Monograph 14, pp 411–431

Deer WA, Howie RA, Zussman J (1992) An introduction to the rock-forming minerals, 2nd edn. Longman House, Burnt Mill

Deer WA, Howie RA, Wise WS, Zussman J (2004) Framework silicates: silica minerals, feldspathoids and the zeolites, Rock-forming minerals Volume 4B (2nd ed). The Geological Society of London, 982 pp

Dunphy JM, Fletcher IR, Cassidy KF, Champion DC (2003) Compilation of SHRIMP geochronological data, Yilgarn Craton, Western Australia, 2001–2002. Geoscience Australia Record 2003/15, 139 pp

Duuring P, Hagemann SG, Cassidy KF, Johnson CA (2004) Hydrothermal alteration, ore fluid characteristics, and gold depositional processes along a trondhjemite-komatiite contact at Tarmoola, Western Australia. Econ Geol 99:423–451

Einaudi MT, Hedenquist JW, Inan EE (2003) Sulfidation state of fluids in active and extinct hydrothermal systems: transition from porphyry to epithermal environments. Society of Economic Geologists, Special Publication 10:285–313

Evans KA, Phillips GN, Powell R (2006) Rock-buffering of auriferous fluids in altered rocks associated with the Golden Mile-style mineralization, Kalgoorlie Gold Field, Western Australia. Econ Geol 101: 805–817

Faure G (2001) Origin of igneous rocks: the isotopic evidence. Springer, Berlin-Heidelberg, 496 pp.

Fleet ME (2003) Sheet silicates: micas. Rock-forming minerals Volume 3A, 2nd ed. The Geological Society, London

Fletcher IR, Dunphy JM, Cassidy KF, Champion DC (2001) Compilation of SHRIMP U-Pb geochronological data, Yilgarn Craton, Western Australia, 2000–2001. Geoscience Australia Record 2001/47, 111 pp

Frost BR (1991) Introduction to oxygen fugacity and its petrologic importance. In: Lindsley DH (ed) Oxide minerals: petrologic and magnetic significance. Mineralogical Society of America, Rev Mineral, vol. 25, p. 1–9

Gauthier L (2006) Atlas of Fimiston-style mineralisation paragenesis, Golden Mile gold deposit, Kalgoorlie, W.A. Centre for Exploration Targeting, the University of Western Australia, Perth

Gauthier L, Hagemann S, Robert F (2007) The geological setting of the Golden Mile gold deposit, Kalgoorlie, W.A. In: Bierlein FP, Knox-Robinson CM (eds) Kalgoorlie 2007, old ground, new knowledge, abstracts. Geoscience Australia, Record 2007/14, pp 181–185

Goldfarb RJ, Baker T, Dubé B, Groves DI, Hart CJR, Gosselin P (2005) Distribution, character and genesis of gold deposits in metamorphic terranes. Econ Geol 100th Anniversary Volume, pp 407–450

Golding SD, Groves DI, McNaughton NJ, Mikucki EJ, Sang JH (1990) Sulphur isotope studies. In: Ho SE, Groves DI, Bennett JM (eds.) Gold deposits of the Archaean Yilgarn Block, Western Australia: nature, genesis, and exploration guides. University of Western Australia, Publication 20, pp. 259–262

Goscombe BD, Blewett RS (2009) Plate 1: East Yilgarn Craton metamorphism and strain map. Geoscience Australia Map Series: www.ga.gov.au/data-pubs/maps

Grant JA (1986) The isocon diagram—a simple solution to Gresen's equation for metasomatic alteration. Econ Geol 81:1976–1982

Groves DI (1993) The crustal continuum model for late-Archaean lode-gold deposits of the Yilgarn Block, Western Australia. Mineral Deposita 28:366–374

Hagemann SG, Cassidy KF (2000) Archean orogenic lode gold deposits. SEG Rev 13:9–68

Hallberg JA (1983) Geology and mineral deposits of the Leonora-Laverton area, northeastern Yilgarn Block, Western Australia. Geological Survey of Western Australia Record 1983/8, 140 pp

Ho SE, Bennett JM, Cassidy KF, Hronsky JMA, Mikucki EJ, Sang JH (1990) Fluid inclusion studies. In: Ho SE, Groves DI, Bennett JM (eds.) Gold deposits of the Archaean Yilgarn Block, Western Australia: nature, genesis, and exploration guides. University of Western Australia, Publication 20, pp. 198–211

Holland TJB, Powell R (1998) An internally consistent thermodynamic data set for phases of petrological interest. J Metamorph Geol 16: 309–343

Holland TJB, Powell R (2000) AX—a program to calculate activities of mineral end members from chemical analyses (determined by electron microprobe): www.esc.cam.ac.uk/astaff/holland/ax.html

Krusch P (1903) Beitrag zur Kenntnis der nutzbaren Lagerstätten Westaustraliens. Zeitschrift für praktische Geologie 11:321–331, 369-389

Lanari P, Wagner T, Vidal O (2014) A thermodynamic model for di-trioctahedral chlorite from experimental and natural data in the system MgO-FeO-Al_2O_3-SiO_2-H_2O: applications to P-T sections and geothermometry. Contrib Mineral Petrol 167:968

Larcombe, COG (1913) The geology of Kalgoorlie, Western Australia, with special reference to the ore deposits. Australasian Inst Min Engineers, Melbourne, Monograph, 315 pp

Lindgren W (1906) Metasomatic processes in the gold deposits of Western Australia. Econ Geol 1:530–544

Lister GS, Snoke AW (1984) S-C mylonites. J Struct Geol 6:617–638

Meyer C, Hemley JJ (1967) Wall rock alteration. In: Barnes HL (ed) Geochemistry of hydrothermal ore deposits, 1st edn. Holt, Rinehart and Winston, New York, pp 166–235

Montgomery A (1906) Occurrence of natural gas in the Northern Associated Mine at Kalgoorlie. Annual Report Dept of Mines Western Australia for 1905, pp 98–99

Mueller AG (1990) The nature and genesis of high- and medium-temperature Archaean gold deposits in the Yilgarn Block, Western Australia, including a specific study of scheelite-bearing gold skarn deposits. Dissertation, the University of Western Australia, Perth

Mueller AG (2007) Copper-gold endoskarns and high-Mg monzodiorite-tonalite intrusions at Mt. Shea, Kalgoorlie, Australia: implications for the origin of gold-pyrite-tennantite mineralization in the Golden Mile. Mineral Deposita 42:737–769

Mueller AG (2015) Structure, alteration, and geochemistry of the Charlotte quartz vein stockwork, Mt Charlotte gold mine, Kalgoorlie, Australia: time constraints, down-plunge zonation, and fluid source. Mineral Deposita 50:221–244

Mueller AG (2017) Structural setting of Fimiston- and Oroya-style pyrite-telluride-gold lodes, Paringa South mine, Golden Mile, Kalgoorlie: 1. Shear zone systems, porphyry dykes and deposit-scale alteration zones. Mineralium Deposita online, https://doi.org/10.1007/s00126-017-0747-3

Mueller AG, Muhling JR (2013) Silver-rich telluride mineralization at Mount Charlotte and Au-Ag zonation in the giant Golden Mile deposit, Kalgoorlie, Western Australia. Mineral Deposita 48:295–311

Mueller AG, de Laeter JR, Groves DI (1991) Strontium isotope systematics of hydrothermal minerals from epigenetic Archean gold deposits in the Yilgarn Block, Western Australia. Econ Geol 86:780–809

Mueller AG, Hall GC, Nemchin AA, Stein HJ, Creaser RA, Mason DR (2008) Archean high-Mg monzodiorite-syenite, epidote skarn, and biotite-sericite gold lodes in the Granny Smith-Wallaby district, Australia: U-Pb and Re-Os chronometry of two intrusion-related hydrothermal systems. Mineral Deposita 43:337–362

Mueller AG, Lawrance LM, Muhling J, Pooley GD (2012) Mineralogy and PTX relationships of the Archean Hannan South Au-Cu (Co-Bi) deposit, Kalgoorlie, Western Australia: thermodynamic constraints on the formation of a zoned intrusion-related skarn. Econ Geol 107: 1–24

Mueller AG, Hagemann SG, McNaughton NJ (2016) Neoarchean orogenic, magmatic and hydrothermal events in the Kalgoorlie-Kambalda area, Western Australia: constraints on gold mineralization in the Boulder Lefroy-Golden Mile fault system. Mineralium Deposita online, https://doi.org/10.1007/s00126-016-0665-9

Neumayr P, Walshe J, Hagemann S, Petersen K, Roache A, Frikken P, Horn L, Halley S (2008) Oxidized and reduced mineral assemblages in greenstone belt rocks of the St. Ives gold camp, Western Australia: vectors to high-grade ore bodies in Archaean gold deposits? Mineral Deposita 43:363–371

Phillips GN (1986) Geology and alteration in the Golden Mile, Kalgoorlie. Econ Geol 81:779–808

Powell R, Holland TJB (1994) Optimal geothermometry and geobarometry. Am Mineral 79:120–133

Prider RT (1947) Chloritoid at Kalgoorlie. Am Mineral 32:471–474

Purvis AC (1984) Metamorphosed altered komatiites at Mount Martin, Western Australia—Archaean weathering products metamorphosed at the aluminosilicate triple point. Aust J Earth Sci 31:91–106

Rasmussen B, Mueller AG, Fletcher IR (2009) Zirconolite and xenotime U-Pb constraints on the emplacement of the Golden Mile Dolerite sill and gold mineralization at the Mt Charlotte mine, Eastern Goldfields Province, Yilgarn Craton, Western Australia. Contrib Mineral Petrol 157:559–572

Robert F, Poulsen KH (2001) Vein formation and deformation in greenstone gold deposits. Rev Econ Geol 14:111–155

Rose AW, Burt DM (1979) Hydrothermal alteration. In: Barnes HL (ed) Geochemistry of hydrothermal ore deposits, 2nd edn. Wiley, New York, pp 173–235

Scantlebury GM (1983) The characterization and origin of the gold lodes in and around the Brownhill syncline, Golden Mile, Kalgoorlie, Western Australia. B.Sc. (Honours) thesis, the University of Western Australia, Perth, 90 pp

Sibson RH (1977) Fault rocks and fault mechanisms. J Geol Soc London 133:191–213

Simpson ES (1912) Detailed mineralogy of Kalgoorlie and Boulder with special reference to the ore deposits. In: Simpson ES, Gibson CG (eds) The geology and ore deposits of Kalgoorlie, East Coolgardie Goldfield, Part 1. Geol Survey Western Australia, Bulletin 42, pp 77–151

Skwarnecki MS (1990) The regional setting and genesis of Archaean gold mineralization at Harbour Lights, Leonora, Western Australia. Ph.D. thesis, the University of Western Australia, Perth

Stillwell FL (1929) Geology and ore deposits of the Boulder Belt, Kalgoorlie. Geol Survey Western Australia, Bulletin 94, 110 pp

Tomich SA (1952) Some structural aspects of Kalgoorlie geology. Proc Aust Inst Min Metall 164(165):45–76

Tomich SA (1959) The Oroya Shoot and its relationship to other flatly plunging ore pipes at Kalgoorlie. Proc Aust Inst Min Metall 190: 113–124

Travis GA, Woodall R, Bartram GD (1971) The geology of the Kalgoorlie goldfield. Geol Soc Aust Spec Pub 3:175–190

Tripp G I (2013) Stratigraphy and structure in the Neoarchaean of the Kalgoorlie District, Australia: critical controls on greenstone-hosted gold deposits. Dissertation, James Cook University, Townsville

Wang R, Cudahy T, Laukamp C, Walshe J, Bath A, Mei Y, Young C, Roache TJ, Jenkins A, Roberts M, Barker A, Laird J (2017) White mica as a hyperspectral tool in exploration for the Sunrise Dam and Kanowna Belle gold deposits, Western Australia. Econ Geol 112: 1153–1176

Witt WK (1991) Regional metamorphic controls on alteration associated with gold mineralization in the Eastern Goldfields Province, Western Australia: implications for the timing and origin of Archean lode-gold deposits. Geology 19:982–985

Woodall R (1965) Structure of the Kalgoorlie goldfield. 8th Commonwealth Mining and Metallurgy Congress, Melbourne, pp 71–79